

Review

The Influence of Cutting Technology on Magnetic Properties of Non-Oriented Electrical Steel—Review State of the Art

Maria Dems , Zbigniew Gmyrek and Krzysztof Komeza * 

Institute of Mechatronics and Information Systems, Lodz University of Technology, 90-924 Lodz, Poland; maria.dems@p.lodz.pl (M.D.); zbigniew.gmyrek@p.lodz.pl (Z.G.)

* Correspondence: krzysztof.komeza@p.lodz.pl; Tel.: +48-42-6312571

Abstract: The global drive to reduce energy consumption poses new challenges for designers of electrical machines. Losses in the core are a significant part of losses, especially for machines operating at an increased rotational speed powered by PWM inverters. One of the important problems when calculating core losses is considering the effect of material degradation due to mechanical or laser cutting. To this aim, this paper analyzes and summarizes the knowledge about the sources of material property deterioration and ways of describing this phenomenon. The cited results of material tests indicate the lack of unequivocal relationships allowing us to estimate the degree of material damage and the resulting deterioration of material properties. The main task of this article is to present the state of knowledge on the possibility of taking into account the impact of cutting the core sheets of electric motors on core losses and their impact on the efficiency of the machine. This is a significant problem due to the need to design and manufacture energy-saving electric motors powered with a voltage of 20 to 350 Hz, whose magnetic cores are made of laminates. However, the performed analysis indicates the most important parameters of the cutting process, affecting the degree of material structure destruction. The method of the solution proposed by the authors for core punching and laser cutting, illustrated with a practical example, is also presented.

Keywords: cutting effect; electrical steel sheet specific loss; loss approximation



Citation: Dems, M.; Gmyrek, Z.; Komeza, K. The Influence of Cutting Technology on Magnetic Properties of Non-Oriented Electrical Steel—Review State of the Art. *Energies* **2023**, *16*, 4299. <https://doi.org/10.3390/en16114299>

Academic Editor: Nicu Bizon

Received: 6 May 2023

Revised: 19 May 2023

Accepted: 23 May 2023

Published: 24 May 2023



Copyright: © 2023 by the authors. Licensee MDPI, Basel, Switzerland. This article is an open access article distributed under the terms and conditions of the Creative Commons Attribution (CC BY) license (<https://creativecommons.org/licenses/by/4.0/>).

1. Introduction

To reduce the impact of climate change by reducing energy consumption, the EU implemented, in 2009, a series of energy requirements called Eco-sign. From 1 July 2023, the third phase comes into force, which means that all electric motors with a power of 0.75 kW to 1000 kW must have an energy class corresponding to at least IE3, and motors from 0.12 kW to 0.75 kW must be IE2 class. There are around eight billion electric motors in the EU alone, estimated to account for more than half of the world's electricity consumption. With the assumed lifetime of the motor equal to 15 years, the purchase cost does not usually exceed a few percent of the cost of use. This should result in a different approach to constructing electrical machines, mainly aimed at reducing losses and thus increasing energy efficiency.

Considering the overall effect of the revised regulation [1], the annual savings will increase to 110 TWh by 2030, avoiding around 40 million tons of CO₂ emissions per year.

The Super-Efficient Equipment and Appliance Deployment (SEAD) initiative is outside the European Union and connects countries worldwide to cooperate in promoting energy-saving devices. In addition, the International Energy Agency's 4E Electric Motors Systems Annex works to raise global awareness of the efficiency potential of motor systems and provide guidance and tools to exploit the energy efficiency of new and existing motor systems worldwide.

Figure 1 shows an example of loss distribution in a low-power induction motor for different working frequencies [2]. As can be seen, for machines operating at mains and

lower frequencies, the losses in the core constitute a significant part of the losses, but the losses in the windings prevail. In contrast, for machines operating at an increased frequency, the losses in the core are dominant. In addition, as seen in work [3], the share of core losses in total losses has a slight tendency to increase with the increased rated motor power. In addition, a significant increase in stray load losses should be noted, which are core losses and depend on similar parameters as classic core losses.

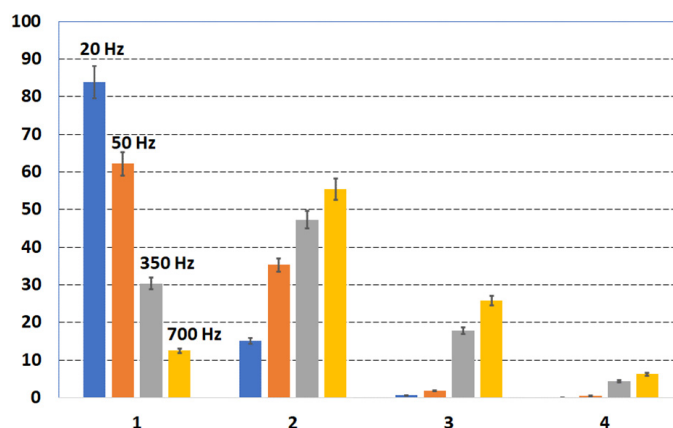


Figure 1. Percentage share of motor losses at nominal load, at 20 Hz, 50 Hz, 350 Hz, and 700 Hz of supply voltage; 1—losses in the winding, 2—losses in the core (fundamental and additional), 3—mechanical losses, 4—other additional losses.

Hence, there is a common interest in both the problem of the exact description of core losses and the search for methods to reduce them.

The creation of cores for electric motors and transformers requires shaping of their geometry. In the case of transformers, relatively simple shapes of core fragments are used, similar to a rectangle or a trapezoid, whereas in the case of electric motor cores, the shape is much more complicated, especially around the slots. It is known that the process of cutting ferromagnetic material is not indifferent to the material's properties. Currently used laminations made of soft ferromagnetic material are not fully isotropic. As a result, changes in the local material properties depend on the angle between the cutting line direction and the laminate rolling direction. The indicated facts became the basis for conducting scientific research, combining the observed adverse effects of cutting with changes in the local properties of the material and its crystallographic and domain structures. Changes in the domain and crystallographic structure as well as the macroscopic properties of soft ferromagnetic materials, resulting from the implementation of the cutting process, have been studied for many years. The first references to the causes of these changes can be found in the works of Bozorth, carried out in the 1940s and 1950s [4]. This was due to the visible differences between the magnetizing currents and losses measured on real models and the values estimated based on approximate models [5–7]. The problem became particularly important after introducing new regulations on the efficiency of electrical machines caused by the desire to reduce electricity consumption.

Analyzing the available literature, it should be noted that additive manufacturing methods are currently being widely developed. As a result of their use, the destruction of the material's internal structure, resulting from the implementation of the mechanical or laser cutting process (manifested by the deterioration of the material's magnetic properties), is avoided. Referring to additive manufacturing methods, a group of works describing research conducted on sintered materials can be identified [8–15], as well as a group of works depicting the research results using laser powder bed fusion technology [16–19]. As the published research results on SMC and LPBF materials indicate, they can be used mainly in motors operating at frequencies of kHz and higher. Then, the low specific iron loss of the material about the Fe–Si laminates, which the authors of this article deal with,

is their undoubted advantage. Similarly, the benefit of this type of solution is the lack of structure destruction caused by the discussed cutting technologies.

Unfortunately, the disadvantage of cores made of these materials is the long time needed to produce them. While in the case of prototype solutions, it is acceptable, in mass production, it is unacceptable.

According to the authors, the central area is currently addressing the problems associated with the mass production of electric motors. Therefore, further considerations will focus on two cutting technologies: mechanical and laser. According to the authors' knowledge regarding the mass production of low-loss electric motors, the issue of the impact of stator and rotor sheet metal processing on the size of the iron losses is still attractive. These motors operate in the frequency range from several dozen to several hundred Hz, so their stator and rotor cores are made of Fe–Si laminates.

Several studies have shown that machining, especially cutting, significantly affects core losses. Therefore, this paper analyzes and summarizes the knowledge about the sources of material property deterioration and ways of describing this phenomenon. Subsequently, Section 2 presents the results of research conducted in two areas. The first area of research concerns the presence of residual stresses and the local increase in the material's microhardness; the second describes the results of grain structure morphology and domain structure changes. Section 3 contains an analysis of the analytical models used by the researchers to reproduce changes in induction and material-specific loss in areas close to the cut edge. Section 4 briefly summarizes the introduction to FEM simulation of the models of changes in material parameters due to the cutting presented in Section 3. Section 5 briefly describes the approximation method proposed by the authors in paper [20]. Applied approximation makes it possible to determine the material's average (equivalent) properties, depending on the frequency, induction, and actual width of the motor core fragment. To illustrate the effectiveness of its operation, the authors used it in the calculations carried out for a low-power induction motor operating at 50 Hz and 350 Hz, the core of which was shaped using two technologies: mechanical punching and laser cutting. Combining the proposed approximation with the high-accuracy analytical model of the induction motor enabled the exact determination of the motor's operational parameters.

2. Morphology of Grains and Measurements of the Macroscopic Properties of Strips Undergoing the Cutting Process

Based on the research results described below, it should be stated that the applied cutting technologies change the structure and properties of the material to varying degrees. Commonly used technologies that significantly influence these changes include guillotine, punching, and laser cutting. In addition to the technologies mentioned above that are in common use, other less invasive technologies are used, which have a relatively small impact on these changes, including water jet cutting and wire electrical discharge machining (spark erosion). Their disadvantage is the long time needed to cut an element of a given shape, eliminating them from mass production. At the same time, they are used during experimental research, making it possible to cut out elements with minimal invasion, essentially changing their magnetic properties to a small extent. Scientific research conducted in this area is multi-directional, starting from studies of changes in the structure of magnetic domains and ending with morphological changes and residual stress distributions. The presented state of the art is in two areas. The first refers to the presence of residual stresses and local changes in the microhardness of the material, and the second is related to changes in the morphology of the grains and the structure of the magnetic domains.

Tests of the presence and distribution of residual stresses and changes in material microhardness include:

- testing the presence of elastic and plastic deformations and residual stress distributions inside the cut material. The research results available in the literature indicate a relatively strong influence of internal stresses on changes in macroscopic material properties. As Ossart points out, plastic deformations predominate at a relatively

short distance from the cut edge [7]. Research conducted by many researchers on the deterioration of the material's macroscopic properties caused by the presence of stresses leads to the conclusion that plastic deformation causes a significant deterioration of the magnetic properties of electrical steels. This is particularly evident at low strains (typically from 0 to 5%) and low and medium magnetic field amplitudes (up to a few kA/m) [21–23]. Stresses below the elastic limit can either increase or decrease the macroscopic material parameters, such as the magnetic permeability of a material. This conclusion is supported by research results presented by Daem et al. [23]. This generally depends on whether the material exhibits positive or negative magnetostriction, but exceptions have been reported by Allia et al. [24]. Once the stress crosses the elastic limit and plastic flow occurs, magnetic permeability reduces rapidly. As demonstrated by Maeda et al., tensile stresses are generated near the cut edge, whereas compressive stresses are further away from the cut edge [25]. Analyzing the fundamental work [4], we conclude that the more the stress exceeds the elastic limit, the more the initial and maximum permeability decrease. The study of the impact of plastic deformations and residual stresses on changes in material properties must be supplemented with an answer to the question about the distance from the cut edge where deformations and strains occur. The answer to this question can be found, for example, in the work of Xiong et al. [26]. The authors show the dependence of residual stress in the cut edge zone as a function of the distance from the cut edge. At the same time, they determine the increase in stresses about those that occur in the undamaged part of the material. This distance was defined as close to the one in which mechanical hardening of the material occurs (increase in microhardness). Cutting technology is known to affect the size and area of residual stress. Therefore, research has been conducted in the guillotine and laser cutting field. For guillotine-cut material, Cao et al. presented the research results on the width of the area where residual stress occurs [27]. According to them, the range of rapid stress changes can be defined as 100–150 μm , while more minor changes are observed up to 400 μm . In the entire range, the residual stress value changes from about 350 MPa to about 100 MPa. Maeda et al. show that laser cutting also “generates” residual stresses, with values comparable to those occurring during guillotine cutting [25]. Omura et al. conducted extensive research on the impact of material microhardness (in the undamaged zone) and strip thickness on the maximum plastic strain value [28]. They showed that the harder the material, the lower its maximum hardening on the cut edge and the smaller the area of increased microhardness. Examining the influence of the thickness of the strip, they found that the thicker the strip, the greater the maximum value of plastic strain and the wider the area of increased hardness. Fujisaki et al. researched the presence of plastic and elastic stresses in ferromagnetic strips [29]. The authors presented the results of tests and simulations concerning guillotine cutting, indicating the presence of stresses and the size of the zones where plastic and elastic stresses occur. They concluded that the size of the area where plastic stresses occur is comparable to half the thickness of the tested strip.

- microhardness tests (as known, microhardness is the hardness of a material gauged with instruments using small indenters. It linearly correlates with the tensile strength. This allows cost-effective, non-invasive testing). In work by Hofmann et al., tests were performed for three cutting technologies: guillotine, laser, and spark erosion [30]. When examining the maximum hardening in the cutting zone, it was found that the guillotine causes a rise in hardness by 70%, and the laser causes an increase by 15% with regard to spark erosion cutting. The spark erosion technology essentially does not increase the hardness. At the same time, the authors defined the width of the mechanical hardening zone as 120–150 μm . As described by Araujo et al. [31], microhardness changes in a similar range were registered, while Wenmin et al. in [32] state that this size can be even be defined as reaching 2 mm. On the other hand, the work of A. Pulnikov et al. indicates that the width of the area in which the increase in

microhardness occurs (guillotine cutting) is about 150 μm [33]. In this area, there is an 80% increase in microhardness compared to undamaged material. At the same time, the authors note that the introduction of additional compression applied to the sample causes a slight increase in the maximum microhardness with a simultaneous almost two-fold increase in the width of the area with increased microhardness. In another paper, Pulnikov presents the results of microhardness measurements executed for various electrical steel sheets [34]. He obtained deterioration depth ranges from 0.4 to 2.8 mm, depending on the type and thickness of the material tested. The work carried out by the team of Kurosaki et al. indicated a possible greater range of microhardness changes during guillotine cutting (even up to 350 μm) as well as the possibility of a microhardness increase by 10% during laser cutting (at a distance of up to 150 μm from the edge) [35,36]. Schoppa noted in his research that the width of the area with increased microhardness depends on the silicon content [37]. From other works, it is known that an increase in the silicon content causes an increase in grain size, so one could generalize Schoppa's observations. It should therefore be concluded that the width of the zone with increased microhardness depends on the average grain size. This statement is supported by the results of the research conducted by Schmidt, who defined the zone size as 350 μm , examining a material with 1% silicon content [38]. In materials with a relatively low silicon content (relatively small grains), the size of this zone does not exceed 500 μm . In contrast, it can reach as much as 1–2 mm for materials with somewhat higher content. Omura et al. tested materials with a thickness of 0.35 mm, with a microhardness varying from 154 to 217 [28]. They showed that the material with lower microhardness had a 50% wider zone of microhardness changes resulting from guillotine cutting than the harder material. At the same time, the percentage increase in the maximum microhardness (at the cut edge) of the softer material was 20% higher than for the harder material. This work also described the strip thickness's influence on the zone's width in which the microhardness increase occurred. For the thinner material (0.2 mm), a zone whose width was half that of the thicker material (0.35 mm) was found. In turn, the work of Saleem et al. did not show a significant increase in microhardness as a function of distance for laser-cut material [39]. Belhadj et al., who analyzed the material cut with a laser, reached other conclusions, noting the dependence of changes in properties on the speed of moving the laser beam [40]. It has been shown that for a laser moving at a rate of 6 m/min, the hardening zone reaches 500 μm (the authors performed Vickers hardness tests, obtaining microhardness changes from 140 to 180 HV). When the laser beam moved at a lower speed, i.e., 3 m/min, the width of the hardened zone increased to 2 mm, and the microhardness reached 200 HV. In the literature, we can find the results of research conducted by Baudouin et al. in which the effect of knife clearance on the change in maximum hardening and its range was analyzed [41]. The authors showed that at the cut edge, an increase in microhardness by about 60% is possible, and the content of these changes can reach up to about 800 μm , strongly dependent on the chemical composition of the material. Wang et al. studied the effect of clearance varying from 3 to 10% for a material with a thickness of 0.3 mm, having small grains (27 μm) [42]. It was noticed that the range of microhardness changes occurring at a distance of up to 200 μm from the edge did not essentially depend on clearance, and the maximum increase in microhardness differed by 10%. The authors showed that there is an optimal clearance value for which the maximum hardening is the smallest (this value depends on the grain size). Wu et al. compared the size of the zone with increased microhardness and its maximum value for non-oriented materials cut with a guillotine and stamped [43]. They found that guillotine cutting increased the area where the higher microhardness was measured by 20% and, at the same time, reduced the maximum microhardness value by 10%. By simultaneously examining the changes in plastic deformation for both cases, the authors confirmed the same proportions as for the microhardness curve. Similar research was conducted by Weiss et al. In [44],

the cutting blade wear's influence on the zone's width with increased microhardness and maximum microhardness was described. Materials with a thickness of 0.35 and 0.5 mm, with comparable grain sizes and hardness of the undamaged material, were tested. Studies have shown that cutting with a worn tool causes a 10% increase in microhardness compared to that occurring due to cutting with a sharp blade. A similar result was obtained for four times faster cutting. The width of the area where the increase in microhardness occurs was determined as 0.25 mm for sharp tools and slow cuts and 0.3 mm for worn tools and fast cuts. Research by Ossart et al. indicates a more than two-fold increase in the microhardness of the material (at the cut edge), combining the current microhardness with plastic strain [7]. Although the area of increased microhardness was determined to be about 200 μm from the edge, it was also noticed that even small changes in plastic strain drastically change the macroscopic characteristics of the material, such as the $B-H$ curve. As is known, mechanical hardening generates new dislocations of the crystallographic structure, which, among other things, affect the change in the material's macroscopic properties. The work finds the results of dislocation density and microhardness tests near the cut edge. The range of observed changes was defined as close to 400 μm , which correlates very well with the results of the study conducted by Xiong et al. [45].

Grain morphology and domain structure studies:

- observations of the domain structure. The work by Hofmann et al. contains observations made with the MOKE microscope, indicating that as a result of cutting, a part of the material is magnetically hardened [4]. Spark erosion did not essentially change the domain structure (only a few μm from the edge), and the guillotine cut affected a larger area than the laser cut (even 600 μm for the guillotine), changing the magnetic domain patterns at the same time. For guillotine cutting, patterns were found to form due to plastic deformations and dislocations. The largest deformation occurs in the range of about 150 μm , which correlates well with the size of the zone with increased microhardness. Laser cutting causes a more significant deformation of domain patterns (in an area of similar width) than guillotine cutting, and changes are observed up to 800 μm from the edge. Works by Steentjes et al. [46] and Schoppa et al. [47] analyze the results of macroscopic measurements of material properties. The authors state that spark erosion and water jet cutting are the least invasive cutting technologies, slightly changing the domain structure. As shown in the above works, the choice of cutting technique affects the size of the damaged area. Additionally, Harstick et al. [48] and Regnet et al. [49] indicate that tool wear significantly influences the changes in the crystallographic structure during guillotine cutting. Research conducted by Hubert et al. indicates the impact of plastic deformations on the movement of Bloch walls [50]. The authors emphasize that plastic deformations (due to the increase in the density of dislocations) affect the movement of the walls more intensively than the rotation of the magnetic moments. These locations act as potential barriers that hinder the Bloch wall motion. A similar conclusion was formulated many years earlier, where the author suggested that plastic strains give rise to forces opposing the movement of Bloch walls [51]. Observation with the MOKE microscope allowed Senda et al. to indicate areas containing different formations of magnetic domains than in the part of the material where the effect of cutting is negligible [52]. Reports on the possibility of the appearance of an oxidized layer with a width of several μm having completely different properties were described by Belhadj et al. [40]. They showed that for a 500 μm thick strip, three characteristic areas could be identified: the area up to about 150 μm from the edge, where strip patterns approximately parallel with the sheet plane were observed; an area extending from 150 to 500 μm , where stripe patterns extending in the perpendicular direction with the sheet plane were observed; and an area extending from 500 to 750 μm , where a slight change in the domain patterns in the limited portions was visible. The total width of the place where changes in domain patterns were observed was determined to be 1–1.4 mm from the cut edge.

The analysis of the results of observations with the MOKE microscope, described in [53], leads to similar conclusions. Naumoski et al. links the results of observations of areas with changed domain patterns (created as a result of guillotine cutting) with the results of microhardness measurements, concluding that at a distance of about 200–220 μm from the edge, there is a hardened magnetic zone [54]. In addition, they show, based on magnetic contrast measurements, that the set magnetic zone (with varying degrees of hardening) reaches three to four times deeper into the material than the mechanically hardened zone, reaching as much as 1 mm. According to other researchers, the hardened magnetic zone may extend to a distance of 5 mm [55] or even 10 mm [5]. The research conducted by Naumoski's team presents the results of observations with the MOKE microscope, pointing to an essential aspect regarding the magnetically hardened zone created due to the guillotine and laser cutting [56]. The authors pointed out that the width of this zone (magnetic activity of the material) depends not only on the cutting technology used but also on the intensity of the magnetic field affecting this region. It was noticed that for low external magnetic field strengths (of the order of 100 A/m), the magnetically hardened zone shows relatively weak activity for both cutting techniques in relation to the zones of undamaged material. For somewhat higher magnetic field strengths (of the order of 1600 A/m), in the case of laser cutting, the zone becomes more active (magnetic domains are formed more quickly). For comparison, the authors also showed the same zones after annealing, indicating a very large replication of the domain structure of these zones. An important area of research is exploring the impact of elastic applied tensile stress. A good example is the work carried out by the team of Perevertov et al. [57]. The tests were carried out for tensile stress from 0 to 60 MPa. They showed significant differences in domain patterns and the formation of a complex domain structure at the grain boundary. Cao et al. observed the domain structure at the guillotine-cut edge and at a long distance where the material was not damaged [27]. The undamaged material tested was shown to have 100 μm grains with complicated domain patterns, including 180°-domain and 90°-domain. Most domain patterns are closure domain structures, which can decrease the magnetostatic energy. The change in the domain structure can be observed within the area of 0.3 mm from the edge to the center of the strip. The difference in the domain structure indicates that the residual compressive stress caused by the punching process can change the crystallographic and domain structures near the edge of the sample. Saleem et al. observed grains with slab-like domains near the edge of a laser-cut strip [39]. The authors indicated that at a distance of about 450 μm from the edge, there was a small number of grains with such a structure (this region is treated as magnetically hardened), and from 450 μm to 3000 μm , there was a constant number of grains with such a structure (essentially independent of the distance). At a distance from 3000 μm to 6000 μm , the number of grains with such a structure increased (depending on the distance), while in the zone located over 6000 μm , the number of grains with such a structure stabilized.

- observations of the crystallographic structure. The study conducted by Araujo et al. concerning the material cut with a guillotine and a laser contains the results of the observation of the crystallographic structure in the vicinity of the cut edge [31]. The guillotine cut causes plastic deformation near the cut line to be seen. In contrast, laser cutting does not induce any changes in the grain morphology near the cut line. Similar observations about punching and spark erosion can be found in [32,35,56,58,59]. Comparing the results of the above studies, it was found that punching “generates” plastic deformations much smaller than cutting with a guillotine. At the same time, spark erosion, as with a laser, does not cause plastic deformations. Gmyrek et al. studied material in the form of a 0.5 mm thick strip subjected to guillotine cutting, with grains of an average size of about 100 μm [60]. During the tests, they noticed the presence of grains of a smaller size at a distance of 200–300 μm from the cut edge. The size of this area harmonizes well with the size of the area where the presence of

plastic stresses is observed. An in-depth analysis of changes in the crystallographic structure resulting from guillotine cutting can be found in [41]. The authors indicate the existence of four regions with varying degrees of structure changes (rollover, shear zone, ductile fracture zone, and burr), illustrating it with microscopic observations. Based on the measurements carried out for knife clearance in the range of 2 to 8% of the thickness of the cut strip, its influence on the size of the ductile fracture region and the size of the burr was demonstrated. It was also pointed out that these regions' size depends on the material's chemical composition. Currently, the research subject is studying crystallographic orientations using EBSD technology. In the works of Xiong et al. [26,44] and Bali et al. [61], the results of misorientation angle distributions in the edge zone of the Fe–Si steel after mechanical cutting were presented. The authors showed that crystals set at an angle of 0 and 45–50 degrees dominate at the cut edge, while those set at an angle of 40–55 degrees dominate at a distance greater than 500 µm. The results of the work by Füzér et al. show changes in the structure of the crystallographic lattice occurring due to guillotine cutting. These changes depend on the tool's clearance and cause significant misorientation of the crystals in the damaged area [62]. The authors state that clearance (in the range of 1–7%) significantly affects the size of the area where crystal misorientation occurs. The figures show that the microstructural part in the vicinity of the cutting edge presented by the authors is characterized by a high level of misorientation angles in the range of 2–5 degrees and even more. It indicates that these grains are characterized by increased intensity of mechanical strain associated with high dislocation density. Quoting the authors, it should be stated that the results presented show that the depth of the penetration of residual stresses in the cutting surface area was significantly lower when the shear-cutting process was performed with a smaller cutting clearance. On the other hand, according to the authors, the local misorientation maps show that smaller cutting clearances may lead to higher residual stresses immediately next to the cutting surface. The results also show that a smaller cutting clearance reduces the size of the area affected by shearing.

3. Simulation Models of Changes in Electromagnetic Properties Caused by the Cutting Process of Non-Grain Oriented Electrical Steel Sheets

Models of sheet metal degradation under the influence of punching differ significantly in terms of complexity. The simplest substitute models assume the division of the sheet width into two zones: damage due to cutting and undamaged. However, the problem here is determining the damaged zone's width. This issue has been discussed in detail in the review paper [52,63–65]. Simple models include those presented in the papers [66–68]. In both recent papers [67,68], the authors assume a constant width of the damaged zone. However, although the procedure assumes a constant width of the damaged zone, it does not require its knowledge because samples of different widths are used for the analysis. The authors do not specify what width of the damaged zone corresponds to the obtained results. The averaged magnetization and loss characteristics were measured using two samples of different widths. On this basis, the authors introduce a relationship for a given value of the magnetic field strength H (1).

$$\begin{bmatrix} 1 - \gamma_1 & \gamma_1 \\ 1 - \gamma_2 & \gamma_2 \end{bmatrix} \begin{bmatrix} B_{n-d} \\ B_d \end{bmatrix} = \begin{bmatrix} B_1 \\ B_2 \end{bmatrix} \quad (1)$$

It allows for determining the values of magnetic flux densities $B_{n-d}(H)$ and $B_d(H)$ ($n-d$ for the non-damaged part and d for the damaged part). The coefficient values are determined for the entire measurement series. The coefficients γ_1 and γ_2 correspond to the share of the completely degraded area in the smaller and larger widths sample, respectively. The coefficients are determined using the regression method by comparing the values obtained based on the above relationship and the measurement values. It should be emphasized that the method used does not exactly correspond to the assumption of a

specific width of the degraded zone and the determination of parameters for the degraded and undamaged material.

The magnetization characteristics outside the measurement points are approximated by third-order spline functions (cubic spline), which allows for the appropriate accuracy to be obtained while maintaining the continuity of the derivative. In addition, attention was paid to the correct mapping in the Rayleigh region (for induction values less than 0.2 T), as well as in the full saturation region.

The authors adopted a relatively simple and rarely used loss approximation for the losses in the form of (2), assuming that the c_1 coefficient must be positive.

$$p_{Fe} = c_1 B + c_2 B^2 \quad (2)$$

Despite a simple approximation, the obtained loss curves correspond well to the measured curves after applying a method analogous to the magnetization characteristic. The results were applied to the FEM analysis of the stator core using the specified width of the damaged layer. The stator sheet is wound, so the field is mainly in the yoke. The authors indicate the influence of other factors related to the assembly of the finished engine, such as gluing or welding and core pressing, which cause additional stresses resulting in increased losses in the core. The influence of these factors was taken into account using the work [69].

The papers [70,71] examined non-oriented sheets with a width of 0.2 and 0.35 mm and a width of 5 to 60 mm in a wide frequency range. Based on experimental tests, the width of the degraded zone was determined to equal: for a sheet of 0.2 mm thickness, 1.739 mm and a sheet of 0.35 mm thickness, 2.044 mm. In paper [71], tests were also carried out for sheets cut using a water jet, and although this method of cutting is considered the least invasive, the width of such a zone was determined to be 1.5 mm. However, it should be noted that such a significant width of the damaged zone is not confirmed in other works. It was stated that the influence of the abrasive waterjet cutting on electromagnetic properties is minimal and can essentially be neglected in the case of the non-alloyed grade [47,72,73].

Since the papers use the model with the width of the degraded zone, the peak magnetic polarization J_p for a sample with a width of w is (3)

$$J_p(w) = J_{p,n-d} - \left(J_{p,n-d} - J_{p,d} \right) \frac{2L_d}{w} \quad (3)$$

where L_d is the width of the degraded zone, the index $n-d$ refers to the non-degraded part, and d refers to the degraded part.

Similarly for losses (4)

$$p_h(J, w) = p_{h,n-d}(J_{n-d}) + (p_{h,d}(J_d) - p_{h,n-d}(J_{n-d})) \frac{2L_d}{w} \quad (4)$$

Thus, as you can see, the authors assume the degradation affects hysteresis losses. A similar relationship was assumed for anomalous losses, while eddy current losses were considered independent of the cutting effect.

Many more papers assume a continuous dependence on the impact of material degradation on electromagnetic parameters as a function of the distance from the cut edge. The reliance of degradation on distance from the cut edge is exponential in most cases; only in a few instances are polynomials or other relationships used. These works are presented chronologically and grouped according to the approximation method.

In work [74], a unique model of the motor core was used only with cut-out stator slots and such excitation of the windings placed in the slots so that the magnetic flux was mainly concentrated in the area of the teeth. A sheet with a thickness of 0.65 mm was tested. The adopted model assumes an exponential change in permeability, decreasing from the tooth's center toward the cutting line.

$$\mu_d = \mu_{n-d} e^{-\alpha x/d} \quad (5)$$

where x is the distance from the tooth's center, and $2d$ is the width of the tooth.

From this dependence and the assumption of a simple relation for core losses as a function of induction, the dependence on average losses in a tooth as a function of induction results in

$$p_{Fe} = \frac{1 - e^{-\eta\alpha}}{\eta\alpha} p_{n-d} \quad p_{n-d} = aB^\eta \quad (6)$$

where α is the parameter obtained from the measurement for the damaged sample.

An important conclusion from that paper was that the most significant degradation effect for the magnetization characteristic is visible within the saturation knee at 1.3 T. In comparison, the differences significantly decrease above the induction of 1.6 T.

In paper [75], the tests were carried out for four different grades of non-oriented sheet metal with a thickness of 0.5 mm, characterized by very different grain sizes (from 120 to 17 μm) and other silicon content (from 3.2 to less than 0.2%). The measurement of the induction distribution in the sheet was carried out using probes of various widths wound through holes with a diameter of 0.5 mm for the average induction of 1 T and 1.5 T and the frequency of 50 Hz. Based on the study of the induction distribution, an approximation model was developed that best reflects the character of distributions of the form

$$B(x) = \frac{a}{(1 + e^{b-cx})^{1/d}} \quad (7)$$

The parameters change significantly depending on the sheet's grain size and Si content. These changes, however, are quite chaotic and did not allow for the development of a coherent description linking these parameters with the degradation of magnetic properties.

The papers [76,77] examined non-oriented electrical sheet steel with a thickness of 0.3 mm cut with a guillotine and a laser. It was assumed that the maximum reduction in sheet permeability due to cutting depends on the material properties and cutting parameters and has a constant value while maintaining these parameters. Similarly, the value of the width of the degraded zone was assumed to be constant. However, it was mentioned that this value depends on both the material parameters, such as sheet thickness or grain size, as well as the parameters of the cutting tool, mainly the clearance between the punching elements and the blade's geometry. Therefore, the distribution of changes in permeability in the material as a function of the distance from the cut edge x is described by the dependency:

$$\Delta\mu(H, x) = \Delta\mu_{amp}(H)\eta(x) \quad (8)$$

where $\eta(x)$ is a parabolic function

$$\eta(x) = 1 - \frac{x}{\delta} - a\frac{x}{\delta}\left(1 - \frac{x}{\delta}\right) \quad (9)$$

Taking the above into account, an expression describing the loss density distribution in the form (10) was obtained

$$p_{Fe}(x) = a_2(x)J(H, x)^2f + a_1(1 + a_3J(H, x)^{a_4})J(H, x)^2f^2 + a_5J(H, x)^{1.5}f^{1.5} \quad (10)$$

In this expression, only the coefficient a_2 corresponding to hysteresis losses depends on the distance x from the cut edge.

In article [78], as in [74], a very interesting experimental model of the machine was presented with only the stator slots cut out, and a uniform sheet metal rotor was used. Such a model made it possible to avoid difficulties related to the exact determination of losses in the rotor cage. It is necessary to precisely determine the cage temperature and the phenomena associated with the uneven distribution of the current density in the cage bar. It should be noted, however, that the lack of rotor slots results in the omission of losses

related to the mutual movement of the grooved stator and the rotor. A sheet of 0.5 mm thickness was used in the tests.

$$p_{Fe}(x, J(x), f) = s_h(x) \left(1 + (r-1) \frac{J_{\min}(x)}{J_p(x)}\right) J_p(x)^{\alpha(x) + \beta(x) J_p(x)} f + s_e \sum_{n=1}^{\infty} [J_{p,n}(x)^2 (nf)^2] + s_{exc}(x) \sum_{n=1}^{\infty} [J_{p,n}(x)^{1.5} (nf)^{1.5}] \quad (11)$$

The specific losses of the electrical sheet, depending on the distance from the cut edge, are described by a relationship (11) containing five parameters s_h , s_e , s_{exc} , α , and β , depending on the type of material. The parameter r is an additional parameter that considers the increase in losses due to the ellipticity of the magnetic field. As can be seen, higher harmonics of the field resulting from the slotting of the stator and the saturation of the local part of the magnetic circuit were also taken into account in the relationship.

In work [30], the tests were carried out for a sheet with a thickness of 0.342 mm, an average grain size of 96 μm , and a Si content of 2.8%. The article states that the magnetic induction distribution in the sheet can be obtained by correcting the induction distribution obtained for a homogeneous material based on solving the problem by taking into account the eddy currents by the function of the degradation coefficient depending on the distance from the cut edge and the induction modulus (12). The degradation coefficient is much less than unity for small inductions and takes the value of 1 for flux density greater than 1.8 T.

$$B(x, z, t) = \zeta_d(x, |B|) B(z, t) \quad (12)$$

In article [79], sheet samples with a thickness of 0.35 and 0.2 mm, and additionally, a CoFe sheet were tested. In this work, a description of the interaction for a sample cut on both sides was introduced

$$\mu_d(x, B) = \mu_{n-d}(B) + [1 - \mu_{n-d}(B)] \left[2\delta\alpha(B) \left(1 - e^{-\frac{1}{\delta\alpha(B)}}\right) - e^{-\frac{1}{\delta\alpha(B)}} \right] \quad (13)$$

$$\delta = \frac{e}{w}$$

where w is the sample width, e denotes the sheet thickness, and α is a degradation parameter to be determined.

As is known, a certain magnetic anisotropy characterizes a non-grain oriented sheet; samples cut both by and perpendicular to the rolling direction were tested.

In articles [80–82], permeability is described as a function (14)

$$\mu_{r,d}(H) = \mu_{r,n-d}(H) \left(1 - e^{-\frac{H}{\tau}}\right) + 1 \quad (14)$$

where

$$\tau(x) = \frac{\gamma}{1 - \left(\frac{x}{d}\right)^c} \quad (15)$$

and x is the distance from the cut edge, and d is the width of the damaged zone.

Power losses in the material can be approximated by:

$$p_{Fe} = (k_d x + q) k_h \left(\frac{B}{B_0}\right)^\alpha \left(\frac{f}{f_0}\right) + k_{ec} \left(\frac{B}{B_0}\right)^2 \left(\frac{f}{f_0}\right)^2 \quad (16)$$

Thus, only the hysteresis losses are modified. Based on the measurements, the width of the damaged zone was assumed to be equal to 1 mm. The application is limited to FEM field analysis in a ring sample.

In papers [83–85], a sheet with a thickness of 0.5 mm was tested. The local permeability value at a distance x from the cut edge is given by (17):

$$\mu(H, x) = \mu_{n-d}(H) - \Delta\mu(H) e^{-ax} \quad (17)$$

where $\Delta\mu(H)$ and a are parameters determined from measurements.

Thus, the losses are

$$\begin{aligned} w_{Fe}(B, x) &= \left(K_{h0} + \Delta K_h(B)e^{-bx} \right) B^{\alpha(B)} f + K_e B^2 f^2 + \\ & (K_{ex0} + \Delta K_{ex}(B)e^{-cx}) B^{1.5} f^{1.5} \\ \Delta K_h(B) &= b_1 B^3 + b_2 B^2 + b_3 B + b_4 \\ \Delta K_{ex}(B) &= c_1 B^3 + c_2 B^2 + c_3 B + c_4 \end{aligned} \quad (18)$$

The parameters are calculated from the measurement curves using the least squares method. As in one of the previous works, the tests were carried out for a model machine with a rotor without slots but only for a stationary rotor, i.e., in the conditions of a pulsating field. The phenomena associated with the formation of higher harmonics in the rotating slotted rotor were modeled by supplying the motor with voltage at different frequencies. As an example of application, the FEM analysis over time was used, including rotation for a 37 kW induction motor; however, the simulation results were not compared with the measurements on a real motor.

Article [86] analyzes a non-oriented sheet with a thickness of 0.5 mm. The density of losses in the core is approximated by the relationship (19), where it was assumed that cutting affects only hysteresis losses.

$$\begin{aligned} p_h(x) &= K_{h0} \left(1 + \frac{c_0}{1+c_1 d(x)} e^{-dx} \right) B(x, H)^\alpha f \\ d(x) &= \exp((-B(x, H) + c_2)^{c_3}) \end{aligned} \quad (19)$$

In Formula (19), the impact of punching is represented by the coefficients c_1 , c_2 , c_3 , and d , determined by fitting them to the measurement data. The loss model was applied to the prototype IE4 efficiency class induction motors analysis rated at 2.2 kW. The work's advantage is comparing experimental results for the motor without and with heat treatment (annealing).

In article [87], a sheet with a thickness of 0.5 mm was tested. Permeability is approximated by (20)

$$\mu(H, x) = \mu_{n-d}(H) \left(1 - \frac{2}{\pi} \mu_p e^{\frac{-x}{a\mu}} \left(\arctan\left(\frac{H}{H_1}\right) - \arctan\left(\frac{H}{H_2}\right) \right) \right) \quad (20)$$

based on four coefficients, and losses

$$p_{Fe}(B, x) = k_{h0} \left(1 + k_p e^{\frac{-x}{ap}} \right) f B^{\alpha_0} + k_{e0} (1 + x_{10} B^{x_{20}}) f^2 B^2 \quad (21)$$

based on six coefficients. Application was in PMSM and SynRel. As in the previous article, losses with and without heat treatment calculated using FEM and the treatment effect model were compared.

Article [88] describes the permeability in the damaged material using an exponential degradation profile (22).

$$v(B, x) = v_{n-d}(B) (1 - e^{-\tau x}) + v_d(B) e^{-\tau x} \quad (22)$$

Similarly, the loss density in the damaged core is described using an exponential profile. Unlike other works, it assumes that the treatment affects both hysteresis and eddy current losses.

$$\begin{aligned} p_{Fe}(B, x) &= (k_{h,n-d} (1 - e^{-\tau_h x}) + k_{h,d} e^{-\tau_h x}) B^2 f + \\ & (k_{e,n-d} (1 - e^{-\tau_e x}) + k_{e,d} e^{-\tau_e x}) B^2 f^2 \end{aligned} \quad (23)$$

Adopting an exponential model of changes in material properties required the use of appropriate Gauss–Jacobi quadrature in implementing the finite element method.

Using the SST apparatus, paper [89] performed tests on a wide range of non-oriented materials with thicknesses from 0.1 to 0.35 mm. The approximation formula for losses is quite complicated (24)

$$w_{Fe} = a_1 B_m^{\alpha+\beta} f + \frac{\pi^2 d^2 \gamma}{6\rho} B_m^2 f^2 (1 + a_3 B_m^{a_4}) + a_5 (B_m f)^{1.5} \tag{24}$$

and contains five coefficients. As a result of tests for samples of different widths, it was found that a linear approximation for a_1 , a_3 , and a_5 or an exponential one for a_3 can be used.

Article [90] presents a slightly different approach. Magnetization is modeled using the Langevin function (25)

$$M = \chi_V H \quad M = M_s \left[\coth\left(\frac{H}{a}\right) - \frac{a}{H} \right] \tag{25}$$

where M_s is the saturation magnetization, which we assume does not depend on mechanical effects, while a is a material parameter dependent on magnetic susceptibility

$$a = \frac{M_s}{3\chi_0} \tag{26}$$

The Gumbel distribution describes the magnetic susceptibility of damaged material

$$\chi_0 = (\chi_{n-d} - \chi_d) \exp\left[-\exp\left(-\frac{x-d_0}{\beta_0}\right)\right] + \chi_d \tag{27}$$

When calculating losses, hysteresis and anomalous loss factors are described by different Gumbel distributions—the approximation error concerns measurements at several percent and is applied to PMSM.

Further works [91,92] have attempted to link material degradation with electromagnetic properties. Sablik’s anhysteretic model based on dislocation density was used to consider plastic deformation. As expected, implementing the model in an induction motor shows the degradation of the magnetic flux density near the punching edge due to the effect of plastic deformation. The parameters of the Sablik model are identified by fitting the model to the measured magnetization curves for different levels of elastic stresses and plastic strains. Unfortunately, the model considered magnetization and not losses in the core. The authors also indicate selected types of this model. The investigation develops the research direction based on which a mechanical phenomenon arises with the subsequent change in magnetic parameters.

As a supplement to the cited works, Table 1 contains selected papers not mentioned so far concerning the inclusion of the impact of cutting in the process of simulating the operation of electric machines. The works are arranged according to the type of the tested machine. Machine specifications, contents, and conclusions are briefly listed for each item.

Table 1. Selected papers not mentioned so far concerning the inclusion of the impact of cutting in the process of simulating the operation of electric machines.

Paper	Motor Type	Short Description	Contents and Conclusions
[93]	PMSM	Four-pole motor with stator outer diameter of 150 mm, embedded magnets.	Time-stepping finite element analysis of the induced voltage during rotation. The stator sheet at the cut edge was divided into six layers from the edge, and the appropriate identified BH curve was used for each.
[94]	PMSM	Analysis of a motor with a rated power of 219 W and an outer stator diameter of 90 mm.	The impact of cutting on the flux distribution was investigated, emphasizing the impact on local distributions. A slight effect of cutting on the electromagnetic torque of the machine was found, but with a significant effect on the efficiency.

Table 1. Cont.

Paper	Motor Type	Short Description	Contents and Conclusions
[95]	PMSM	An 8-pole/9-slot motor with a rated power of 10 kW for a rotational speed of 19,000 rpm and a stator outer diameter of 70 mm.	An increase in core losses was found. A reduction in an overall efficiency of 1% was found, which in high-performance aeronautical applications cannot be overlooked.
[96]	PMSM	Four-pole PMSM motor with 90 mm stator outer diameter.	Core losses were studied. A local magnetic material model was used in the FEM simulation. Using a local model of the magnetic material enabled realistic prediction of the magnetic induction distribution and the specific distribution of losses in the tested electrical machine.
[97]	PMSM	Six-pole pairs, peak power 85 kW, maximum rotational speed 10,000 rpm.	Accounting for the effects of punching resulted in a 30% increase in rotor and stator losses. The authors also indicate the impact of punching on the mechanical characteristics obtained.
[98]	BLDC PM	A brushless DC surface-mounted PM motor with a rated power of 26 kW and a stator outer diameter of 137 mm was tested.	Core losses in the frequency range from 200 to 1400 Hz were investigated. A significant increase in core losses of up to 32% was found due to the cutting and assembly effect. However, this increase in losses could be removed by applying annealing.
[99]	PMSM	A permanent magnet synchronous 4-pole machine with a rated power of 150 W and a rotational speed of 6000 rpm.	The simulation results showed that the consideration of material damage at the cut edge in the calculation of the motor size under consideration is of immense importance for accurate result.
[100]	PMSM	An interior rotor fractional horsepower permanent magnet synchronous machine featuring 12 stator slots and 2 p = 8 poles was investigated.	The article concerns the optimization of the design of this motor, taking into account the effects of cutting. The stator sheet at the cut edge was divided into four layers from the edge. The authors emphasize that the optimal constructions were very sensitive to changes in the manufacturing process.
[101]	PMSM	PMSM motor with a rated power of 30 kW, a rated speed of 2860 rpm, and a maximum speed of 14,000 rpm, embedded magnets, and three pairs of poles.	The influence of the cutting on the magnetization curve was taken into account. The authors emphasize that the significant impact of punching is mainly observed for small-size machines and small-width magnetic circuit elements.
[102]	SFHP PM	The analysis of sub-fractional horsepower SFHP machines with a power of about 800 mW.	This paper investigates and compares the three stator lamination stacks' selected magnetic performance parameters (i.e., cogging torque, hysteresis torque, and iron losses). Due to their small dimensions, such machines are particularly vulnerable to the degradation effects associated with cutting.
[103]	SFHP BL PM	SFHP single-phase brushless permanent magnet motor often found in automotive fan applications, 10-pole motor with stator outer diameter of 85 mm. The rotor has surface-mounted bread-loaf-shaped magnets.	The effect of cutting on cogging torque was investigated. It has been found that the change in the magnetic properties of the teeth caused by punching causes the formation of additional ones and low-order harmonics in the machine cogging torque with an amplitude comparable to the fundamental harmonics.
[104]	PMSM	The machine under study is a medium-size PMSM with one layer of V-shape magnets and a double-layered aluminum stator winding. Motor rated 100 kW for electric vehicle, 4-pole, outer diameter 213 mm.	The impact of cutting on torque and losses was investigated. Core material degradation can increase losses by up to 35%. Torque reduction can reach 1%. Driving cycle tests show a 21% increase in core loss.

Table 1. Cont.

Paper	Motor Type	Short Description	Contents and Conclusions
[105]	PMSM	PMSM with stator outer diameter of 290 mm, rated speed 2750 rpm.	For the FEM simulation, the authors compared single-layer and multi-layer models. The authors state that cutting has negligible effect on the torque ripple. The calculated core loss difference due to cutting was 8%.
[34]	IM	A four-pole induction machine with an external diameter of the stator core of 89 mm and an internal diameter of the rotor core of 20.5 mm is considered.	In addition to examining the impact of cutting on the basic parameters of an induction motor, the work also examined the effects on equivalent inductances used in the circuit modeling of the motor.
[106]	IM	The investigated machine is a small squirrel cage induction machine with the following basic parameters: three phases, two poles, wye connection; the output power is 600 W, the rated speed is 2840 rpm, and the supply voltage is 400 V at 50 Hz.	The influence of cutting on the parameters of an induction motor was investigated. The relative difference between measured and simulated parameters was: for efficiency at a nominal load of 0.6%, current at a nominal load of about 2.4%, and total losses at about 1.5%.
[107]	IM	Analogous as above.	Additionally, the impact of annealing was investigated, allowing for an increase in efficiency by 1.5% for the rated power load.
[108]	IM	An industrial induction motor rated 7.5 kW using 0.5 mm thin sheet, four poles.	FEM simulations indicated an increase of up to 51% in the iron losses and up to 13% in the copper losses at partial load as an effect of cutting.
[109]	IM	Two poles induction machine with a rated power of 600 W at 2846 rpm.	Optimization with the genetic algorithm of the induction motor core slot shapes, considering the effects of cutting. The most significant difference between the basic sizes of the optimized flute shapes with and without considering the cutting effects is about 0.3 mm.
[110]	DS-AFIM	Double-stator axial-flux induction machine, total active length 103.41 mm, outer torus diameter 220 mm.	The torque capability of the model appeared to decrease by 1.3%, and a significant increase in the core losses was observed.
[111]	IM	An induction motor with 5.5 kW power, three phases, four poles, and fan cooling (380 V, 50 Hz, 1500 r/min) was used in the tests.	The study of the impact of punching on the parameters of the induction motor was supported by using an artificial neural network. The measured motor efficiency at 50 Hz and nominal load for punching was 86.81%, while for laser cutting, it was 85%.
[112]	SR	A synchronous reluctance motor with a rated power of 230 kW at 6000 rpm and 37.5 kW at a maximal speed of 18,000 rpm.	A comparison of manufacturing effects on two solutions (radial-rib rotor and multi-innerrrib one). While in most of the analyzed cases, the cutting effect leads to a decrease in efficiency, in the case of the tested machine, it can work the opposite way thanks to increasing the inductance ratio.
[72]	SR	Six-pole reluctance motor with stator outer diameter equal to 120 mm.	Only the stator packages were tested, showing a significant effect of cutting. The additional losses due to cutting decrease with increasing frequency despite the significant increase in total losses. For machine operation at 400 Hz, an additional 50% core loss is expected.

4. Consideration of the Cutting Effect in the FEM Simulation

A separate area of the application of FEM to consider the cutting effect attempts to combine the analysis of mechanical phenomena related to punching with a change in electromagnetic parameters. One such article is the work [7]. However, subsequent studies

have shown that the impact of cutting on mechanical properties extends much further than the change in hardness of the material resulting from mechanical deformation. A critical approach to describing mechanical–electromagnetic phenomena can be found in the papers [113,114]. Paper [115] presents the influence of stresses on the phenomena in the core of a permanent magnet motor. It uses the measured magnetization and loss characteristics of the sheet under tension. In the electromagnetic FEM simulation, the effect of stress is considered by using the BH characteristic measured for a given state of stress. This approach is possible if the stresses are caused by, for example, placing the core in the housing. However, the phenomena are different for cutting because they result from plastic deformations arising during cutting, not the core elements' permanent stress. Similar considerations are presented in article [29]. This paper attempts to consider the plastic deformation caused by the cutting process numerically simulated to determine the electromagnetic effects of this phenomenon. However, the area of influence defined by plastic deformation is much smaller than the area of degradation of electromagnetic properties. In general, it can be said that this area remains open for research.

When simulating the operation of an electric machine using FEM, considering the influence of the cutting effect on electromagnetic properties, three approaches are possible [116], shown in Figure 2.

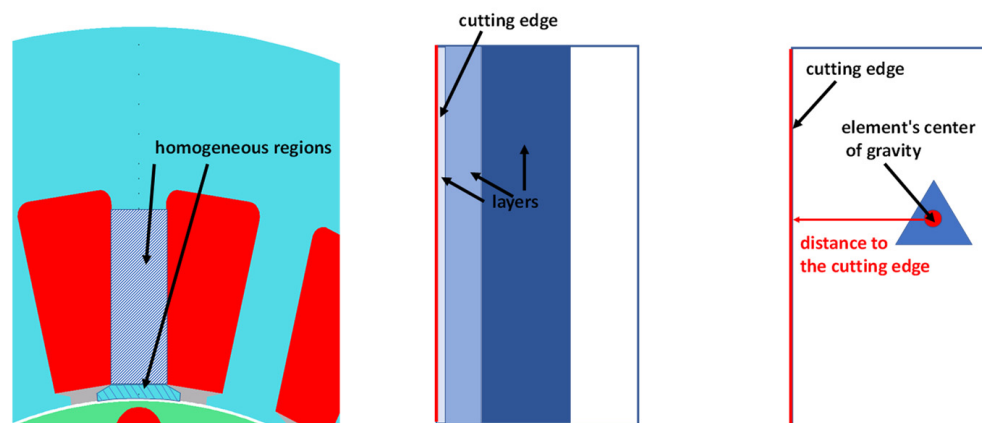


Figure 2. Review of methods for taking into account changes in the electromagnetic parameters of the core material under the influence of cutting in the FEM simulation.

The first is to apply to each area, e.g., a stator tooth, averaged parameters determined considering the width of a given element. This approach was used, for example, in [30,61,78,108,112]. The second is dividing the solution area into layers with different properties [34,78,85,93,104–108,110,117–119]. Since these layers are usually narrow, it creates a problem in the construction of the mesh, forcing the use of small-sized elements because otherwise, similarly to the air gap, degenerate elements with too sharp angles are created. For example, for a small motor with an outer diameter of 150 mm, six layers of small width were used at the edges of the cut [93]. The third way is to assign material properties to the element resulting from the distance of the center of gravity of the element from the nearest edge of the cut [85,88,91,94,96,99,103,120–122]. The last two articles used third-order elements instead of the commonly used linear elements. For linear elements, the induction inside the element is constant. Therefore, it is enough to specify the parameters for the center of gravity of the element. The induction distribution inside the element as a derivative is a quadratic function for the third-order elements. Therefore, calculating the elements' matrix requires using an appropriate number of points where material parameters are also calculated. The use of higher-order elements allows for fewer elements, but this does not significantly affect the cost of the solution due to the greater number of variables for the element.

5. An Example of Determining the Operating Characteristics of an Induction Motor, Taking into Account the Proposed Approximation of the Properties of the Motor Core Material

The authors' work [123] contains the results of calculations of operational characteristics for two low-power induction motors. These motors are characterized by relatively small dimensions, defined by shaft heights of 56 mm and 71 mm. The analyzed motors operate in the frequency range from 10 Hz to 350 Hz and have a core made of M470-50A sheet metal with a thickness of 0.5 mm (mechanical punching was used). The calculations were made using an analytical model based on the equivalent diagram of an induction motor, considering non-linear phenomena occurring in the motor, such as saturation of the magnetic circuit and skin effect in the rotor bars. When calculating both the magnetizing current and the fundamental iron losses in the teeth and the motor yoke, the sheet metal's averaged (equivalent) magnetization and specific iron loss characteristics were used. The averaged (equivalent) material characteristics were determined based on measurements of rectangular samples (at the fundamental frequency), with a width corresponding to the real dimensions of the teeth and the stator yoke, cut at different angles about the rolling direction. In contrast, additional losses in the core caused by higher magnetic field harmonics were determined using the characteristics measured for a sample with a constant width of 10 mm at frequencies from 50 Hz to several kHz.

Article [20] discusses the practical method of approximating iron loss in sheet metal, considering the effect of laser and guillotine cutting. Assuming the phenomena arising in the sheet under the influence of cutting, and especially the uneven distribution of the magnetic flux along the width of the sheet, the iron loss was approximated by the relation

$$p_{Fe} = k_h f B^\alpha + k_e f^2 B^\beta \quad (28)$$

The procedure is carried out according to the following sequential steps. First, whether Formula (28) can be correctly applied to a given core material is checked. For this purpose, we check the linearity of the expression

$$\frac{p_{Fe}}{f} = \frac{k_h f B^\alpha + k_e f^2 B^\beta}{f} = k_h B^\alpha + k_e B^\beta f = c_h + c_e f \quad (29)$$

for a series of constant flux density B values.

The thus obtained c_h and c_e coefficients for the available induction range are approximated using the power function (30)

$$c_h = k_h B^\alpha \quad c_e = k_e B^\beta \quad (30)$$

The tested induction and frequency ranges are divided into subranges to obtain high approximation accuracy. This procedure is carried out for selected sample widths. The coefficients are then approximated by a second-order polynomial, which was chosen for the accuracy of the approximation (31)

$$\begin{aligned} k_h &= c_1 w^2 + c_2 w + c_3 & \alpha &= c_4 w^2 + c_5 w + c_6 \\ k_e &= c_7 w^2 + c_8 w + c_9 & \beta &= c_{10} w^2 + c_{11} w + c_{12} \end{aligned} \quad (31)$$

where w is the width of the part.

Sets of 12 coefficients (31) for each frequency and induction subrange are then used in analytical modeling to determine the properties of a given motor element depending on its width between the cut edges. For each type of electrical sheet, these coefficients should be determined based on measurements of the magnetizability and loss characteristics made for this type of sheet, for samples with a minimum width (e.g., 4 mm) with a practically completely degraded structure and with a maximum width (e.g., 60 mm) where the inactive zone almost does not affect the parameters of sheet metal, punched at an angle of 0 and 90 degrees to the sheet rolling direction, for several selected frequency ranges [124,125].

As a result, a method was obtained to approximate the iron loss characteristics as a function of three variables—magnetic induction, frequency, and sample width. The correctness of the proposed method was checked by comparing the measured and approximated material characteristics both for M270-35A and M460-50A materials, for samples with a width of 4 mm to 60 mm, cut with both a guillotine and a laser, at frequencies up to 4000 Hz.

Based on the measurement results obtained for samples at a frequency of 4000 Hz, iron loss characteristics of samples for higher frequencies (up to 14,400 Hz) were determined by approximation. These characteristics for a rectangular, laser-cut sample with a width of 10 mm were compared with the measurements of iron loss characteristics for a laser-cut ring sample with diameters of 400/420 mm at frequencies ranging from 4000 Hz to 14,400 Hz. The excellent agreement of the results allowed us to determine the loss characteristics for other sample widths in the mentioned frequency range, both for the samples cut with a guillotine and a laser.

Then, these characteristics were used in the analytical calculations of the induction motor operating parameters. It should be emphasized that in the analytical calculations of the magnetic voltages and fundamental losses in the teeth and stator yoke of the motor, as well as additional losses (pulsation and surface losses), were included the actual dimensions of the motor's magnetic circuit elements and the penetration depth of higher harmonics of the magnetic field to the teeth of the stator and rotor. In this way, the real dimensions of the individual parts of the motor's magnetic circuit were considered. This allowed for a more accurate determination of the magnetic voltage drops on the circuit fragments and a more accurate calculation of the fundamental and additional iron losses (pulsation and surface losses). Operating characteristics were calculated for two identical motors with a shaft height of 90 mm, working at a frequency of 50 Hz and 350 Hz, with the core punched in the first motor and the laser cut in the second. The basic electromagnetic parameters of these motors are listed in Table 2.

Table 2. The parameters of the investigated induction motors.

Parameter		Value
Number of pole pairs	(-)	2
Stator core outer diameter	(mm)	134
Stator core inner diameter	(mm)	77
Core length	(mm)	120
Number of stator slots	(-)	24
Number of rotor slots	(-)	30
Stator tooth mean width	(mm)	5.5
Rotor tooth mean width	(mm)	3.5
Stator yoke height	(mm)	9.5
Rotor yoke height	(mm)	12.3

The calculation results were compared with the measurement results for the tested machines. Figures 3 and 4 show the characteristics of the current in the stator winding, total losses, core losses, and efficiency of the motor, with both punched and laser-cut cores as a function of the load torque. The analyzed motors were tested at 50 Hz and 350 Hz. Two groups of material characteristics of the M270-35A sheet were used: the first group was measured for a laser-cut toroidal sample with a 10 mm wide yoke; the second group was obtained as a result of approximation for the width corresponding to the actual dimensions of individual fragments of the core (based on the results of measurements made for samples of different widths, cut with a guillotine and a laser), using the method proposed by the authors [20]. All calculated motor operating characteristics were compared with those measured.

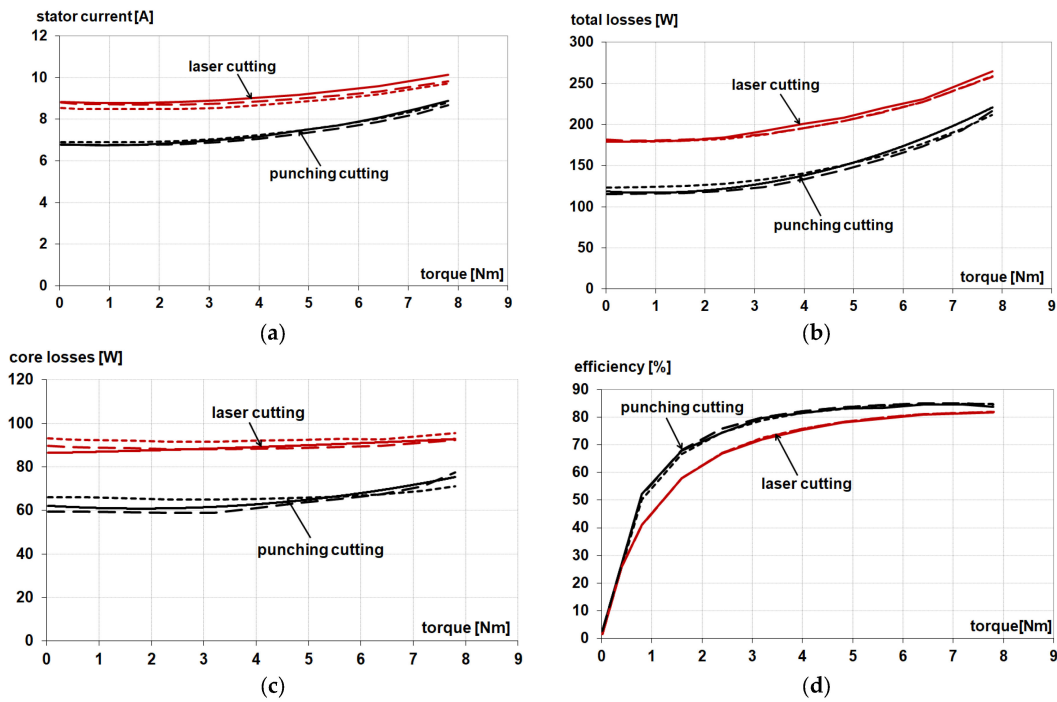


Figure 3. The measured (solid line) characteristics of the stator current (a), total losses (b), core losses (c), and motor efficiency (d). Calculation results obtained with the use of the material characteristics measured for the toroidal samples with a width of 10 mm (point line) and using authors' approximation [20] (dashed line). Measurements and calculations were carried out for the supply frequency of 50 Hz.

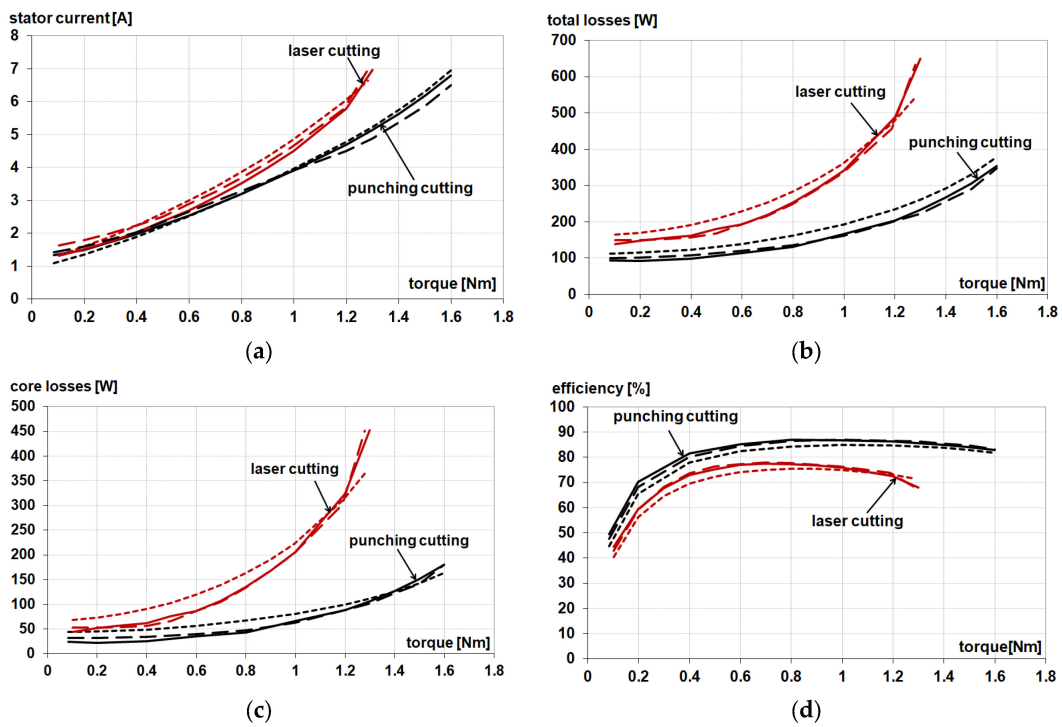


Figure 4. The measured (solid line) characteristics of the stator current (a), total losses (b), core losses (c), and motor efficiency (d). Calculation results obtained with the use of the material characteristics measured for the toroidal samples with a width of 10 mm (point line) and using authors' approximation [20] (dashed line). Measurements and calculations were carried out for the supply frequency of 350 Hz.

Then, the calculation results were compared with the measurement results for the tested motors. Table 3 summarizes the electromagnetic parameters of the motor determined for the characteristics measured for a specimen with a constant width (10 mm), and specimen with a width corresponding to the cores' actual dimensions (listed in Table 2), at 350 Hz and electromagnetic torque 1.3 Nm.

Table 3. Electromagnetic parameters of the motor determined for the characteristics measured for a specimen with a constant width, and specimen with a width corresponding to the cores' actual dimensions at 350 Hz (listed in Table 2), electromagnetic torque 1.3 Nm.

Parameter	Punching Cutting			Laser Cutting		
	Measured	Calculated for Width of 10 mm	Calculated for Actual Width	Measured	Calculated for Width of 10 mm	Calculated for Actual Width
motor shaft power (W)	1398	1398	1398	1377	1377	1377
stator winding current (A)	5.14	5.24	4.89	6.98	6.69	6.92
stator teeth induction (T)	-	0.377	0.374	-	0.382	0.383
stator yoke induction (T)	-	0.428	0.424	-	0.436	0.438
basic core losses (W)	-	28.7	19.2	-	29.6	34.0
additional core losses (W)	-	102.6	82.5	-	336.9	417.4
total core losses (W)	106.5	131.3	101.7	452.2	366.5	451.4
total motor losses (W)	233.4	260.4	222.9	649.3	544.4	633.1
motor efficiency (%)	85.7	84.3	86.2	68.0	71.7	68.5

As the authors of this work clearly demonstrated, for induction motors with relatively small geometric dimensions, it is necessary to use a family of material characteristics determined for a specific width of the magnetic circuit fragment. These characteristics can be approximated using the method proposed by the authors. This method uses the results of measurements made for a small number of rectangular samples of a given width, cut with the indicated technology. A comparison of the results of calculations and measurements shows the acceptable accuracy of the method, which allows the estimation of motor efficiency at the design stage with greater accuracy than other currently used methods.

As can be seen from Table 3, for the tested motor with a guillotine-cut core, the use of material characteristics in the calculations determined for a sample with a constant width (equal to 10 mm) results in losses being obtained in the core that are about 23% higher than those measured, while when performing calculations using the characteristics approximated for the actual dimensions of the motor core elements, the difference between the calculated and measured core losses does not exceed 4.5%. In the case of a laser-cut motor core, the use of material characteristics determined for a sample with a constant width causes differences between the measured and calculated core losses of 19%, while using the characteristics approximated for the actual dimensions of the core elements, it is less than 0.2%.

6. Summary

This article reviews the scientific research results relating to the cutting process's negative impact on a soft ferromagnetic material's micro- and macroscopic properties. The presented analysis refers, first of all, to cutting techniques commonly used in factories: punching, guillotine, and laser cutting. It also indicates the results of research and observa-

tions related to minimally invasive cutting techniques (water cutting and spark erosion) used by scientists to prepare research samples that are practically undamaged in terms of the material. Analyzing the presented test results, we conclude that the significant factors influencing the size and degree of destruction of the area where material changes occur are, above all, the chemical composition of the material and the thickness of the analyzed strips. To a lesser extent, the condition of the tool blades, the cutting speed, and the type of laser used are also factors. The most important conclusion is that the magnetic activity of the material in the damaged zones depends on the applied magnetic field strength. As a result, a variable width of the material zone is actively involved in the magnetization process. This is particularly evident for low magnetic field strengths, usually below 100–200 A/m, for which the width of the magnetically inactive zone varies over a wide range. Generally, the width of the zones of the material with relatively low magnetic activity coincides with the width of the area in which the increase in microhardness is observed. In the case of laser cutting, an area of reduced magnetic activity is observed, even reaching a few mm from the cut edge—such an effect is not observed in the case of guillotine cutting.

Section 3 presents various methods of approximating the magnetic properties of the sheet that change under the influence of cutting. These methods can generally be divided into area-based methods that allow the assigning of averaged parameters determined by the cutting conditions of the machine part and local methods that define these parameters based on the distance from the cutting line. It should be emphasized that these methods are based on measurements of magnetic properties for the sheet subjected to cutting. While in the case of a sheet subjected to stress, it is possible to make the electromagnetic parameters dependent on the stress value, in the case of the punching process, it is not possible to directly link the punching process's parameters with the sheet's resulting electromagnetic parameters. This is due to the large number of parameters defining the punching process and the lack of a reliable physical model describing the phenomenon.

Section 4 presents the methods used to represent the properties of the cut sheet for the FEM simulation.

Section 5 is an original method of determining average (equivalent) material characteristics, considering the deterioration of material properties due to the cutting process. The advantage of this method is its high accuracy while minimizing the number of necessary coefficients. The attached example verified by measurement confirms the adequacy of the method and the analytical model used. Moreover, it can be used in analytical methods and FEM simulations using equivalent parameters.

Author Contributions: Conceptualization, M.D., K.K. and Z.G.; methodology, M.D. and K.K.; software, M.D.; formal analysis, M.D. and K.K.; resources, M.D.; data curation, M.D.; writing—original draft preparation, M.D., K.K. and Z.G.; writing—review and editing, M.D., K.K. and Z.G.; supervision, M.D. and K.K.; project administration, M.D.; funding acquisition, M.D. All authors have read and agreed to the published version of the manuscript.

Funding: This research was funded by National Science Centre (NCN) Poland as part of the Opus-18', grant number 2019/35/B/ST8/00764 "The manufacturing technology impact analysis of small-power high-speed electric motors to refine their analytical models".

Data Availability Statement: Data are available on request due to research founder restrictions.

Conflicts of Interest: The authors declare no conflict of interest.

References

1. European Commission. *Commission Regulation (EU) 2021/341 of 23 February 2021 Amending Regulations (EU) 2019/424, (EU) 2019/1781, (EU) 2019/2019, (EU) 2019/2020, (EU) 2019/2021, (EU) 2019/2022, (EU) 2019/2023 and (EU) 2019/2024 with Regard to Ecodesign Requirements for Servers and Data Storage Products, Electric Motors and Variable Speed Drives, Refrigerating Appliances, Light Sources and Separate Control Gears, Electronic Displays, Household Dishwashers, Household Washing Machines and Household Washer-Dryers and Refrigerating Appliances with a Direct Sales Function*; European Union: Brussels, Belgium, 2021.
2. Dems, M.; Komez, K.; Majer, K. Core losses of the induction motor operating in a wide frequency range supplied from the inverter. *Int. J. Appl. Electromagn. Mech.* **2020**, *64*, 65–82. [[CrossRef](#)]

3. De Almeida, A.T.; Ferreira, F.J.T.E.; Baoming, G. Beyond Induction Motors—Technology Trends to Move Up Efficiency. *IEEE Trans. Ind. Appl.* **2014**, *50*, 2103–2114. [[CrossRef](#)]
4. Bozorth, R.M. *Ferromagnetism*; Wiley-IEEE Press: Hoboken, NJ, USA, 1978. [[CrossRef](#)]
5. Nakata, T.; Nakano, M.; Kawahara, K. Effects of Stress Due to Cutting on Magnetic Characteristics of Silicon Steel. *IEEE Transl. J. Magn. Jpn.* **1992**, *7*, 453–457. [[CrossRef](#)]
6. Moses, A.; Derebasi, N.; Loizos, G.; Schoppa, A. Aspects of the cut-edge effect stress on the power loss and flux density distribution in electrical steel sheets. *J. Magn. Magn. Mater.* **2000**, *215–216*, 690–692. [[CrossRef](#)]
7. Ossart, F.; Hug, E.; Hubert, O.; Buvat, C.; Billardon, R. Effect of punching on electrical steels: Experimental and numerical coupled analysis. *IEEE Trans. Magn.* **2000**, *36*, 3137–3140. [[CrossRef](#)]
8. Darmani, M.A.; Poskovic, E.; Franchini, F.; Ferraris, L.; Cavagnino, A. Manufacturing and Characterization of Novel Multilayer Magnets for Electrical Machine Applications. *IEEE Trans. Energy Convers.* **2022**, *37*, 2398–2407. [[CrossRef](#)]
9. Poskovic, E.; Franchini, F.; Ferraris, L. Effect of the Insulating Layer on the Properties of SMC Inductors. *Appl. Sci.* **2022**, *12*, 8756. [[CrossRef](#)]
10. Kocsis, B.; Fekete, I.; Varga, L.K. Metallographic and magnetic analysis of direct laser sintered soft magnetic composites. *J. Magn. Magn. Mater.* **2020**, *501*, 166425. [[CrossRef](#)]
11. Poskovic, E.; Franchini, F.; Ferraris, L.; Carosio, F.; Grande, M.A. Rapid Characterization Method for SMC Materials for a Preliminary Selection. *Appl. Sci.* **2021**, *11*, 12133. [[CrossRef](#)]
12. Gmyrek, Z.; Lefik, M.; Cavagnino, A.; Ferraris, L. Comparison of the fractional power motor with cores made of various magnetic materials. *Open Phys.* **2017**, *5*, 827–832. [[CrossRef](#)]
13. Ferraris, L.; Franchini, F.; Poskovic, E.; Grande, M.A.; Bidulsky, R. Effect of the Temperature on the Magnetic and Energetic Properties of Soft Magnetic Composite Materials. *Energies* **2021**, *14*, 4400. [[CrossRef](#)]
14. Grande, M.A.; Bidulsky, R.; Cavagnino, A.; Ferraris, L. Investigations on Different Processing Conditions on Soft Magnetic Composite Material Behavior at Low Frequency. *IEEE Trans. Ind. Appl.* **2012**, *48*, 1335–1343. [[CrossRef](#)]
15. Poskovic, E.; Franchini, F.; Ferraris, L.; Grande, M.A. The effect of particle size on the core losses of soft magnetic composites. *AIP Adv.* **2019**, *9*, 035224. [[CrossRef](#)]
16. Khorasani, M.; Gibson, I.; Ghasemi, A.H.; Hadavi, E.; Rolfe, B. Laser subtractive and laser powder bed fusion of metals: Review of process and production features. *Rapid Prototyp. J.* **2023**, *29*, 935–958. [[CrossRef](#)]
17. Slotwinski, J.A.; Garboczi, E.J.; Stutzman, P.E.; Ferraris, C.F.; Watson, S.S.; Peltz, M.A. Characterization of Metal Powders Used for Additive Manufacturing. *J. Res. Natl. Inst. Stand. Technol.* **2014**, *119*, 460–493. [[CrossRef](#)]
18. Zhao, X.; Wang, T. Laser Powder Bed Fusion of Powder Material: A Review. *3D Print. Addit. Manuf.* **2022**. ahead of print. [[CrossRef](#)]
19. Guan, J.; Wang, Q. Laser Powder Bed Fusion of Dissimilar Metal Materials: A Review. *Materials* **2023**, *16*, 2757. [[CrossRef](#)]
20. Dems, M.; Komez, K.; Szulakowski, J. Practical Approximation of Sheet Losses Taking into Account the Guillotine and Laser Cutting Effect. *Energies* **2023**, *16*, 2831. [[CrossRef](#)]
21. Hug, E.; Hubert, O.; Clavel, M. Influence of the plastic anisotropy on the magnetic properties of a nonoriented 3% silicon iron. *J. Appl. Phys.* **1996**, *79*, 4571–4573. [[CrossRef](#)]
22. Hug, E.; Hubert, O.; Clavel, M. Some aspects of the magnetomechanical coupling in the strengthening of nonoriented and grain-oriented 3% SiFe alloys. *IEEE Trans. Magn.* **1997**, *33*, 763–771. [[CrossRef](#)]
23. Daem, A.; Sergeant, P.; Dupré, L.; Chaudhuri, S.; Bliznuk, V.; Kestens, L. Magnetic properties of silicon steel after plastic deformation. *Materials* **2020**, *13*, 4361. [[CrossRef](#)] [[PubMed](#)]
24. Allia, P.; Celasco, M.; Ferro Milone, A.; Masoero, A.; Stepanescu, A. Theory of the remanence in grain-oriented Si–Fe sheets in presence of external stresses. *IEEE Trans. Magn.* **1981**, *17*, 2863–2865. [[CrossRef](#)]
25. Maeda, A.; Jin, Y.; Kuboki, T. Light press of sheet metal edge for reducing residual stress generated by laser cutting considering mechanical properties and intensity of residual stress. *J. Mater. Process. Technol.* **2015**, *225*, 178–184. [[CrossRef](#)]
26. Xiong, X.; Hu, S.; Dang, N.; Hu, K. Effect of stress-relief annealing on microstructure, texture and hysteresis curve of mechanically cut non-oriented Fe–Si steel. *Mater. Charact.* **2017**, *132*, 239–247. [[CrossRef](#)]
27. Cao, H.; Hao, L.; Yi, J.; Zhang, X.; Luo, Z.; Chen, S.; Li, R. The influence of punching process on residual stress and magnetic domain structure of non-oriented silicon steel. *J. Magn. Magn. Mater.* **2016**, *406*, 42–47. [[CrossRef](#)]
28. Omura, T.; Zaizen, Y.; Fukumura, M.; Senda, K.; Toda, H. Effect of hardness and thickness of nonoriented electrical steel sheets on iron loss deterioration by shearing process. *IEEE Trans. Magn.* **2015**, *51*, 2005604. [[CrossRef](#)]
29. Fujisaki, K.; Hirayama, R.; Kawachi, T.; Satou, S.; Kaidou, C.; Yabumoto, M.; Kubota, T. Motor core iron loss analysis evaluating shrink fitting and stamping by Finite-Element Method. *IEEE Trans. Magn.* **2007**, *43*, 1950–1954. [[CrossRef](#)]
30. Hofmann, M.; Naumoski, H.; Herr, U.; Herzog, H.-G. Magnetic Properties of electrical steel sheets in respect of cutting: Micromagnetic analysis and macromagnetic modeling. *IEEE Trans. Magn.* **2016**, *52*, 2000114. [[CrossRef](#)]
31. Araujo, E.G.; Schneider, J.; Verbeken, K.; Pasquarella, G.; Houbaert, Y. Dimensional effects on magnetic properties of Fe–Si steels due to laser and mechanical cutting. *IEEE Trans. Magn.* **2010**, *46*, 213–216. [[CrossRef](#)]
32. Wenmin, S.; Jing, L.; Changyi, L. Effect of cutting techniques on the structure and magnetic properties of a high-grade non-oriented electrical steel. *J. Wuhan Univ. Technol.-Mater. Sci. Ed.* **2014**, *29*, 1246–1251. [[CrossRef](#)]

33. Pulnikov, A.; Baudouin, P.; Melkebeek, J. Induced stresses due to the mechanical cutting of non-oriented electrical steels. *J. Magn. Magn. Mater.* **2003**, *254–255*, 355–357. [[CrossRef](#)]
34. Pulnikov, A. Modification of Magnetic Properties of Non Oriented Electrical Steels by the Production of Electromagnetic Devices. Ph.D. Dissertation, Ghent University, Ghent, Belgium, 2004.
35. Kurosaki, Y.; Mogi, H.; Fujii, H.; Kubota, T.; Shiozaki, M. Importance of punching and workability in non-oriented electrical steel sheets. *J. Magn. Magn. Mater.* **2008**, *320*, 2474–2480. [[CrossRef](#)]
36. Gmyrek, Z.; Kucharska, B. Investigation of local properties of the Fe-Si alloy subjected to mechanical and laser cutting. *Arch. Electr. Eng.* **2023**, *in press*.
37. Schoppa, A.P. Einfluss der Be- und Verarbeitung auf Die Magnetischen Eigenschaften von Schlussgeglühtem, Nichtkornorientiertem Elektrobund. Ph.D. Dissertation, Rheinisch-Westfälischen Technischen Hochschule, Aachen, Germany, 2001. (In German).
38. Schmidt, K.H. Influence of punching on the magnetic properties of electric steel with 1% silicon. *J. Magn. Magn. Mater.* **1976**, *2*, 136–150. [[CrossRef](#)]
39. Saleem, A.; Alatawneh, N.; Rahman, T.; Lowther, D.A.; Chromik, R.R. Effects of laser cutting on microstructure and magnetic properties of non-orientation electrical steel laminations. *IEEE Trans. Magn.* **2020**, *56*, 6100609. [[CrossRef](#)]
40. Belhadj, A.; Baudouin, P.; Breaban, F.; Deffontaine, A.; De Wulf, M.; Houbaert, Y. Effect of laser cutting on microstructure and on magnetic properties of grain non-oriented electrical steels. *J. Magn. Magn. Mater.* **2003**, *256*, 20–31. [[CrossRef](#)]
41. Baudouin, P.; De Wulf, M.; Kestens, L.; Houbaert, Y. The effect of the guillotine clearance on the magnetic properties of electrical steels. *J. Magn. Magn. Mater.* **2003**, *256*, 32–40. [[CrossRef](#)]
42. Wang, Z.; Li, S.; Cui, R.; Wang, X.; Wang, B. Influence of grain size and blanking clearance on magnetic properties deterioration of non-oriented electrical steel. *IEEE Trans. Magn.* **2018**, *54*, 2000607. [[CrossRef](#)]
43. Wu, F.; Zhou, L.; Soulard, J.; Silvester, B.; Davis, C. Quantitative characterisation and modelling of the effect of cut edge damage on the magnetic properties in NGO electrical steel. *J. Magn. Magn. Mater.* **2022**, *551*, 169185. [[CrossRef](#)]
44. Weiss, H.A.; Leuning, N.; Steentjes, S.; Hameyer, K.; Andorfer, T.; Jenner, S.; Volk, W. Influence of shear cutting parameters on the electromagnetic properties of non-oriented electrical steel sheets. *J. Magn. Magn. Mater.* **2017**, *421*, 250–259. [[CrossRef](#)]
45. Xiong, X.; Hu, S.; Hu, K.; Zeng, S. Texture and magnetic property evolution of non-oriented Fe-Si steel due to mechanical cutting. *J. Magn. Magn. Mater.* **2016**, *401*, 982–990. [[CrossRef](#)]
46. Steentjes, S.; Kameyer, K.; Vogt, S.; Bednarz, M.; Volk, W.; Dierdorf, J.; Hirt, G. Influence of material processing steps annealing and cutting on magnetic materials' properties relevant for electrical machine design. In Proceedings of the Conference Forming Technology Forum, Herrsching, Germany, 19–20 September 2013; pp. 1–6.
47. Schoppa, A.; Louis, H.; Pude, F.; Von Rad, C. Influence of abrasive waterjet cutting on the magnetic properties of non-oriented electrical steels. *J. Magn. Magn. Mater.* **2003**, *254–255*, 370–372. [[CrossRef](#)]
48. Harstick, H.M.S.; Ritter, M.; Riehemann, W. Influence of punching and tool wear on the magnetic properties of nonoriented electrical steel. *IEEE Trans. Magn.* **2014**, *50*, 6200304. [[CrossRef](#)]
49. Regnet, M.; Kremser, A.; Reinlein, M.; Szary, P.; Abele, U. Influence of cutting tool wear on core losses and magnetizing demand of electrical steel sheets. In Proceedings of the 9th International Electric Drives Production Conference (EDPC), Esslingen, Germany, 3–4 December 2019; pp. 1–6. [[CrossRef](#)]
50. Hubert, O.; Hug, E. Influence of plastic strain on magnetic behaviour of non-oriented Fe-3Si and application to manufacturing test by punching. *Mater. Sci. Technol.* **1995**, *11*, 482–487. [[CrossRef](#)]
51. De Barr, A.E. *Soft Magnetic Materials Used in Industry*; Chapman & Hall: London, UK, 1959.
52. Senda, K.; Ishida, M.; Nakasu, Y.; Yagi, M. Influence of shearing process on domain structure and magnetic properties of non-oriented electrical steel. *J. Magn. Magn. Mater.* **2006**, *304*, e513–e515. [[CrossRef](#)]
53. Takezawa, M.; Kitajima, K.; Morimoto, Y.; Yamasaki, J.; Kaido, C. Effect of strain by mechanical punching on nonoriented Si-Fe electrical sheets for a nine-slot motor core. *IEEE Trans. Magn.* **2006**, *42*, 2790–2792. [[CrossRef](#)]
54. Naumoski, H.; Maucher, A.; Vandenbossche, L.; Jacobs, S.; Herr, U.; Chassang, X. Magneto-optical and field-metric evaluation of the punching effect on magnetic properties of electrical steels with varying alloying content and grain size. In Proceedings of the IEEE 4th International Electric Drives Production Conference (EDPC), Nuremberg, Germany, 30 September–1 October 2014; pp. 1–9. [[CrossRef](#)]
55. Siebert, R.; Wetzig, A.; Beyer, E.; Betz, B.; Gruenzweig, C.; Lehmann, E. Localized investigation of magnetic bulk property deterioration of electrical steel. In Proceedings of the 3rd Electric Drives Production Conference (EDPC), Nuremberg, Germany, 29–30 October 2013; pp. 60–64. [[CrossRef](#)]
56. Naumoski, H.; Riedmüller, B.; Minkow, A.; Herr, U. Investigation of the influence of different cutting procedures on the global and local magnetic properties of non-oriented electrical steel. *J. Magn. Magn. Mater.* **2015**, *392*, 126–133. [[CrossRef](#)]
57. Perevertov, O.; Thielsch, J.; Schafer, R. Effect of applied tensile stress on the hysteresis curve and magnetic domain structure of grain-oriented transverse Fe-3%Si steel. *IEEE Trans. Magn.* **2015**, *385*, 358–367. [[CrossRef](#)]
58. Emura, M.; Landgraf, F.; Ross, W.; Barreta, J. The influence of cutting technique on the magnetic properties of electrical steels. *J. Magn. Magn. Mater.* **2003**, *254*, 358–360. [[CrossRef](#)]

59. Bulín, T.; Švábenská, E.; Hapla, M.; Ondrkšek, E.; Schneeweiss, O. Influence of laser cutting and punching on magnetic properties of electrical steel M470-50A. In Proceedings of the 25th Anniversary International Conference on Metallurgy and Materials, Brno, Czech Republic, 25–27 May 2016; pp. 670–675.
60. Gmyrek, Z.; Cavagnino, A.; Ferraris, L. Estimation of the Magnetic properties of the damaged area resulting from the punching process: Experimental research and FEM modeling. *IEEE Trans. Ind. Appl.* **2013**, *49*, 2069–2077. [[CrossRef](#)]
61. Bali, M.; Muetze, A. Modeling the effect of cutting on the magnetic properties of electrical steel sheets. *IEEE Trans. Ind. Electron.* **2016**, *64*, 2547–2556. [[CrossRef](#)]
62. Füzér, J.; Dobák, S.; Petryshynets, I.; Kollar, P.; Kovac, F.; Slota, J. Correlation between cutting clearance, deformation texture, and magnetic loss prediction in non-oriented electrical steels. *Materials* **2021**, *14*, 6893. [[CrossRef](#)]
63. Bali, M.; Muetze, A. The Degradation Depth of Non-grain Oriented Electrical Steel Sheets of Electric Machines Due to Mechanical and Laser Cutting: A State-of-the-Art Review. *IEEE Trans. Ind. Appl.* **2019**, *55*, 366–375. [[CrossRef](#)]
64. Bali, M.; Muetze, A. The degradation depth of electrical steel sheets due to mechanical and laser cutting. In Proceedings of the 2017 IEEE 11th International Symposium on Diagnostics for Electrical Machines, Power Electronics and Drives (SDEMPED), Tinos, Greece, 29 August–1 September 2017; pp. 544–549. [[CrossRef](#)]
65. Manescu Paltanea, V.; Paltanea, G.; Gavrilă, H.; Nemoianu, I.V. Estimation of the Damaged Zone Width due to Mechanical Cutting on High Quality Non-Oriented Steels. In Proceedings of the 2018 International Symposium on Fundamentals of Electrical Engineering (ISFEE), Bucharest, Romania, 1–3 November 2018; pp. 1–4. [[CrossRef](#)]
66. Lewis, N.; Anderson, P.; Hall, J.; Gao, Y. Power Loss Models in Punched Non-Oriented Electrical Steel Rings. *IEEE Trans. Magn.* **2016**, *52*, 7300704. [[CrossRef](#)]
67. Bali, M.; Gersem, H.D.; Muetze, A. Determination of Original Nondegraded and Fully Degraded Magnetic Properties of Material Subjected to Mechanical Cutting. *IEEE Trans. Ind. Appl.* **2016**, *52*, 2297–2305. [[CrossRef](#)]
68. Bali, M.; Gersem, H.D.; Muetze, A. Determination of Original Nondegraded and Fully Degraded Magnetic Characteristics of Material Subjected to Laser Cutting. *IEEE Trans. Ind. Appl.* **2017**, *53*, 4242–4251. [[CrossRef](#)]
69. Miyagi, D.; Aoki, Y.; Nakano, M.; Takahashi, N. Effect of Compressive Stress in Thickness Direction on Iron Losses of Nonoriented Electrical Steel Sheet. *IEEE Trans. Magn.* **2010**, *46*, 2040–2043. [[CrossRef](#)]
70. Manescu Paltanea, V.; Paltanea, G.; Nemoianu, I.V. Degradation of Static and Dynamic Magnetic Properties of Non-Oriented Steel Sheets by Cutting. *IEEE Trans. Magn.* **2018**, *54*, 2001705. [[CrossRef](#)]
71. Manescu (Paltanea), V.; Paltanea, G.; Ferrara, E.; Nemoianu, I.V.; Fiorillo, F.; Gavrilă, H. Influence of mechanical and water-jet cutting on the dynamic magnetic properties of NO Fe-Si steels. *J. Magn. Magn. Mater.* **2020**, *499*, 166257. [[CrossRef](#)]
72. Selema, A.; Ibrahim, M.N.; Sergeant, P. Non-destructive electromagnetic evaluation of material degradation due to steel cutting in a fully stacked electrical machine. *Energies* **2022**, *15*, 7862. [[CrossRef](#)]
73. Winter, K.; Liao, Z.; Ramanathan, R.; Axinte, D.; Vakil, G.; Gerada, C. How non-conventional machining affects the surface integrity and magnetic properties of non-oriented electrical steel. *Mater. Des.* **2021**, *210*, 110051. [[CrossRef](#)]
74. Kedous-Lebouc, A.; Cornut, B.; Perrier, J.C.; Manfé, P.; Chevalier, T. Punching influence on magnetic properties of the stator teeth of an induction motor. *J. Magn. Magn. Mater.* **2003**, *254–255*, 124–126. [[CrossRef](#)]
75. Ahmet, P.; Sezer, E.; Naim, D. Mathematical model for cutting effect on magnetic flux distribution near the cut edge of non-oriented electrical steels. *Comput. Mater. Sci.* **2008**, *43*, 1066–1068. [[CrossRef](#)]
76. Vandenbossche, L.; Jacobs, S.; Henrotte, F.; Hameyer, K. Impact of cut edges on magnetization curves and iron losses in e-machines for automotive traction. *World Electr. Veh. J.* **2010**, *4*, 587–596. [[CrossRef](#)]
77. Steentjes, S.; Pfingsten, G.; Hameyer, K. An Application-Oriented Approach for Consideration of Material Degradation Effects Due to Cutting on Iron Losses and Magnetizability. *IEEE Trans. Magn.* **2014**, *50*, 7027804. [[CrossRef](#)]
78. Vandenbossche, L.; Jacobs, S.; Jannot, X.; McClelland, M.; Saint-Michel, J.; Attrazic, E. Iron loss modelling which includes the impact of punching, applied to high-efficiency induction machines. In Proceedings of the 2013 3rd International Electric Drives Production Conference (EDPC), Nuremberg, Germany, 29–30 October 2013; pp. 1–10. [[CrossRef](#)]
79. Kedous-Lebouc, A.; Messal, O.; Youmssi, A. Joint punching and frequency effects on practical magnetic characteristics of electrical steels for high-speed machines. *J. Magn. Magn. Mater.* **2017**, *426*, 658–665. [[CrossRef](#)]
80. Goldbeck, G.; Cossale, M.; Kitzberger, M.; Bramerdorfer, G.; Andessner, D.; Amrhein, W. Numerical Implementation of Local Degradation Profiles in Soft Magnetic Materials. In Proceedings of the 2018 XIII International Conference on Electrical Machines (ICEM), Alexandroupoli, Greece, 3–6 September 2018; pp. 1037–1043. [[CrossRef](#)]
81. Cossale, M.; Kitzberger, M.; Goldbeck, G.; Bramerdorfer, G.; Andessner, D.; Amrhein, W. Local Degradation in Soft Magnetic Materials: A Simplified Modeling Approach. *IEEE Trans. Ind. Appl.* **2019**, *55*, 5897–5905. [[CrossRef](#)]
82. Goldbeck, G.; Cossale, M.; Kitzberger, M.; Bramerdorfer, G.; Andessner, D.; Amrhein, W. Incorporating the Soft Magnetic Material Degradation to Numerical Simulations. *IEEE Trans. Ind. Appl.* **2020**, *56*, 3584–3593. [[CrossRef](#)]
83. Sundaria, R.; Nair, D.G.; Lehikoinen, A.; Arkkio, A.; Belahcen, A. Loss Model for the Effects of Steel Cutting in Electrical Machines. In Proceedings of the 2018 XIII International Conference on Electrical Machines (ICEM), Alexandroupoli, Greece, 3–6 September 2018; pp. 1260–1266. [[CrossRef](#)]
84. Sundaria, R.; Nair, D.G.; Lehikoinen, A.; Arkkio, A.; Belahcen, A. Effect of Laser Cutting on Core Losses in Electrical Machines—Measurements and Modeling. *IEEE Trans. Ind. Electron.* **2020**, *67*, 7354–7363. [[CrossRef](#)]

85. Sundaria, R.; Lehtikoinen, A.; Arkkio, A.; Belahcen, A. Effects of Manufacturing Processes on Core Losses of Electrical Machines. *IEEE Trans. Energy Convers.* **2021**, *36*, 197–206. [[CrossRef](#)]
86. Seo, U.-J.; Kim, D.-J.; Chun, Y.-D.; Han, P.-W. Mechanical Cutting Effect of Electrical Steel on the Performance of Induction Motors. *Energies* **2020**, *13*, 6314. [[CrossRef](#)]
87. Mohammadi, A.A.; Zhang, S.; Pop, A.-C.; Gyselinck, J.J.C. Effect of Electrical Steel Punching on the Performance of Fractional-kW Electrical Machines. *IEEE Trans. Energy Convers.* **2022**, *37*, 1854–1863. [[CrossRef](#)]
88. Gürbüz, I.T.; Martin, F.; Billah, M.M.; Belahcen, A.; Rasilo, P. Effective Implementation of the Effect of Electrical Steel Sheet Cutting into Finite-Element Simulation. In Proceedings of the 2022 IEEE 20th Biennial Conference on Electromagnetic Field Computation (CEFC), Denver, CO, USA, 24–26 October 2022; pp. 1–2. [[CrossRef](#)]
89. Leuning, N.; Schauerte, B.; Schweren, S.; Hameyer, K. Loss Parameter Identification After Cutting for Different Non-Oriented Electrical Steel Grades. *IEEE Trans. Magn.* **2022**, *58*, 2001005. [[CrossRef](#)]
90. Martin, F.; Aydin, U.; Sundaria, R.; Rasilo, P.; Belahcen, A.; Arkkio, A. Effect of Punching the Electrical Sheets on Optimal Design of a Permanent Magnet Synchronous Motor. *IEEE Trans. Magn.* **2018**, *54*, 8102004. [[CrossRef](#)]
91. M'zali, N.; Martin, F.; Sundaria, R.; Henneron, T.; Benabou, A.; Belahcen, A. Finite-Element Modeling of Magnetic Properties Degradation Due to Plastic Deformation. *IEEE Trans. Magn.* **2020**, *56*, 7506704. [[CrossRef](#)]
92. M'zali, N.; Henneron, T.; Benabou, A.; Martin, F.; Belahcen, A. Finite Element Analysis of the Magneto-Mechanical Coupling Due to Punching Process in Electrical Steel Sheet. *IEEE Trans. Magn.* **2021**, *57*, 7401304. [[CrossRef](#)]
93. Sano, H.; Narita, K.; Zeze, E.; Yamada, T.; Kazuki, U.; Akatsu, K. A practical approach for electromagnetic analysis with the effect of the residual strain due to manufacturing processes. In Proceedings of the 2016 IEEE Energy Conversion Congress and Exposition (ECCE), Milwaukee, WI, USA, 18–22 September 2016; pp. 1–7. [[CrossRef](#)]
94. Elfgen, S.; Steentjes, S.; Böhmer, S.; Franck, D.; Hameyer, K. Influences of Material Degradation Due to Laser Cutting on the Operating Behavior of PMSM Using a Continuous Local Material Model. *IEEE Trans. Ind. Appl.* **2017**, *53*, 1978–1984. [[CrossRef](#)]
95. Al-Timimy, A.; Vakil, G.; Degano, M.; Giangrande, P.; Gerada, C.; Galea, M. Considerations on the Effects That Core Material Machining Has on an Electrical Machine's Performance. *IEEE Trans. Energy Convers.* **2018**, *33*, 1154–1163. [[CrossRef](#)]
96. Weiss, H.A.; Tröber, P.; Golle, R.; Steentjes, S.; Leuning, N.; Elfgen, S.; Hameyer, K.; Volk, W. Impact of Punching Parameter Variations on Magnetic Properties of Nongrain-Oriented Electrical Steel. *IEEE Trans. Ind. Appl.* **2018**, *54*, 5869–5878. [[CrossRef](#)]
97. Leuning, N.; Elfgen, S.; Groschup, B.; Bavendiek, G.; Steentjes, S.; Hameyer, K. Advanced Soft- and Hard-Magnetic Material Models for the Numerical Simulation of Electrical Machines. *IEEE Trans. Magn.* **2018**, *54*, 8107008. [[CrossRef](#)]
98. Boubaker, N.; Matt, D.; Enrici, P.; Nierlich, F.; Durand, G. Measurements of Iron Loss in PMSM Stator Cores Based on CoFe and SiFe Lamination Sheets and Stemmed from Different Manufacturing Processes. *IEEE Trans. Magn.* **2019**, *55*, 8100309. [[CrossRef](#)]
99. Goldbeck, G.; Bramerdorfer, G.; Amrhein, W. Impact of Local Degradation in Soft Magnetic Materials on Performance of Permanent Magnet Synchronous Machines. In Proceedings of the 2019 IEEE Energy Conversion Congress and Exposition (ECCE), Baltimore, MD, USA, 29 September–3 October 2019; pp. 3081–3087. [[CrossRef](#)]
100. Bramerdorfer, G. Effect of the Manufacturing Impact on the Optimal Electric Machine Design and Performance. *IEEE Trans. Energy Convers.* **2020**, *35*, 1935–1943. [[CrossRef](#)]
101. Xiao, X.; Müller, F.; Bavendiek, G.; Leuning, N.; Zhang, P.; Zou, J.; Hameyer, K. Modeling of Scalar Dependencies of Soft Magnetic Material Magnetization for Electrical Machine Finite-Element Simulation. *IEEE Trans. Magn.* **2020**, *56*, 7505704. [[CrossRef](#)]
102. Leitner, S.; Gruebler, H.; Muetze, A. Effect of Manufacturing Influences on Magnetic Performance Parameters of Sub-Fractional Horsepower Motors. *IEEE Trans. Magn.* **2021**, *57*, 8205209. [[CrossRef](#)]
103. Abedini Mohammadi, A.; Zhang, S.; Gyselinck, J.; Pop, A.-C.; Zhang, W. Manufacturing-Induced Cogging Torque in Segmented Stator Permanent-Magnet Machines with Respect to Steel Punching. *IEEE Trans. Magn.* **2022**, *58*, 8107808. [[CrossRef](#)]
104. Soltanipour, S.; Thiringer, T.; Lindström, J. Battery Electric Vehicle Performance Evaluation by Considering Punching Effect on PMSM Iron Cores. In Proceedings of the 2022 International Conference on Electrical Machines (ICEM), Valencia, Spain, 5–8 September 2022; pp. 2162–2168. [[CrossRef](#)]
105. Alatawneh, N.; Saleem, A.; Rahman, T.; Lowther, D.A.; Chromik, R. Modelling and analysis of the effects of cutting of core laminations in electric machines. *IET Electr. Power Appl.* **2020**, *14*, 2355–2361. [[CrossRef](#)]
106. Mach, M.; Hajek, V. Model of a small induction machine with effects of manufacturing. In Proceedings of the 2015 International Conference on Electrical Drives and Power Electronics (EDPE), Tatranska Lomnica, Slovakia, 21–23 September 2015; pp. 319–323. [[CrossRef](#)]
107. Mach, M.; Hajek, V. Impact of punching on a small induction motor. In Proceedings of the 2015 IEEE 15th International Conference on Environment and Electrical Engineering (EEEIC), Rome, Italy, 10–13 June 2015; pp. 895–900. [[CrossRef](#)]
108. Burchas, K.; Stening, A.; Souldard, J.; Broddefalk, A.; Lindenmo, M.; Dahlén, M.; Gyllensten, F. Quantifying Effects of Cutting and Welding on Magnetic Properties of Electrical Steels. *IEEE Trans. Ind. Appl.* **2017**, *53*, 4269–4278. [[CrossRef](#)]
109. Martin, M.; Radoslav, C.; Marek, T.; Vitezslav, H. Impact of manufacturing proces on optimal shape of induction machine slots. In Proceedings of the 2017 IEEE International Conference on Environment and Electrical Engineering and 2017 IEEE Industrial and Commercial Power Systems Europe (EEEIC/I&CPS Europe), Milan, Italy, 6–9 June 2017; pp. 1–5. [[CrossRef](#)]
110. Colombo, L.; Tokat, A.; Bitsi, K.; Márquez-Fernández, F.J.; Alaküla, M. Performance Degradation due to Cut Edge Effect for an Axial-Flux Induction Machine. In Proceedings of the 2022 International Conference on Electrical Machines (ICEM), Valencia, Spain, 5–8 September 2022; pp. 1253–1259. [[CrossRef](#)]

111. Bayraktar, Ş.; Turgut, Y. Experimental and statistical analysis of the effects of punching and laser cutting methods on induction motor efficiency and total magnetic losses in silicon lamination sheets. *J. Magn. Magn. Mater.* **2023**, *572*, 170599. [[CrossRef](#)]
112. Credo, A.; Petrov, I.; Pyrhönen, J.; Villani, M. Impact of Manufacturing Stresses on Multiple-Rib Synchronous Reluctance Motor Performance. *IEEE Trans. Ind. Appl.* **2023**, *59*, 1253–1262. [[CrossRef](#)]
113. Daniel, L. Advanced constitutive laws for computational magnetics: The case of magneto-mechanical behaviour. In Proceedings of the 2018 IEEE International Magnetics Conference (INTERMAG), Singapore, 23–27 April 2018; pp. 1–2. [[CrossRef](#)]
114. Aydin, U.; Rasilo, P.; Martin, F.; Singh, D.; Daniel, L.; Belahcen, A.; Rekik, M.; Hubert, O.; Kouhia, R.; Arkkio, A. Magneto-mechanical modeling of electrical steel sheets. *J. Magn. Magn. Mater.* **2017**, *439*, 82–90. [[CrossRef](#)]
115. Fujisaki, K.; Satoh, S. Numerical calculations of electromagnetic fields in silicon steel under mechanical stress. *IEEE Trans. Magn.* **2004**, *40*, 1820–1825. [[CrossRef](#)]
116. Bramerdorfer, G.; Kitzberger, M.; Wöckinger, D.; Koprivica, B.; Zurek, S. State-of-the-art and future trends in soft magnetic materials characterization with focus on electric machine design—Part 2. *TM—Tech. Mess.* **2019**, *86*, 553–565. [[CrossRef](#)]
117. Rasilo, P.; Aydin, U.; Holopainen, T.P.; Arkkio, A. Analysis of iron losses on the cutting edges of induction motor core laminations. In Proceedings of the 2016 XXII International Conference on Electrical Machines (ICEM), Lausanne, Switzerland, 4–7 September 2016; pp. 1312–1317. [[CrossRef](#)]
118. Bali, M.; De Gerssem, H.; Muetze, A. Finite-Element Modeling of Magnetic Material Degradation Due to Punching. *IEEE Trans. Magn.* **2014**, *50*, 745–748. [[CrossRef](#)]
119. Crevecoeur, G.; Sergeant, P.; Dupre, L.; Vandebossche, L.; Van de Walle, R. Analysis of the Local Material Degradation Near Cutting Edges of Electrical Steel Sheets. *IEEE Trans. Magn.* **2008**, *44*, 3173–3176. [[CrossRef](#)]
120. Elfgen, S.; Steentjes, S.; Böhmer, S.; Franck, D.; Hameyer, K. Continuous Local Material Model for Cut Edge Effects in Soft Magnetic Materials. *IEEE Trans. Magn.* **2016**, *52*, 2001304. [[CrossRef](#)]
121. Sundaria, R.; Lehtikoinen, A.; Hannukainen, A.; Arkkio, A. Higher-order finite element modeling of material degradation due to cutting. In Proceedings of the 2017 IEEE International Electric Machines and Drives Conference (IEMDC), Miami, FL, USA, 21–24 May 2017; pp. 1–6. [[CrossRef](#)]
122. Sundaria, R.; Lehtikoinen, A.; Hannukainen, A.; Arkkio, A.; Belahcen, A. Mixed-Order Finite-Element Modeling of Magnetic Material Degradation Due to Cutting. *IEEE Trans. Magn.* **2018**, *54*, 7402008. [[CrossRef](#)]
123. Dems, M.; Gmyrek, Z.; Komezka, K. Analytical Model of an Induction Motor Taking into Account the Punching Process Influence on the Material Properties' Change of Lamination. *Energies* **2021**, *14*, 2459. [[CrossRef](#)]
124. Gmyrek, Z.; Cavagnino, A. Analytical method for determining the damaged area width in magnetic materials due to punching process. In Proceedings of the IECON 2011—37th Annual Conference of the IEEE Industrial Electronics Society, Melbourne, Australia, 7–10 November 2011; pp. 1764–1769. [[CrossRef](#)]
125. Dems, M.; Komezka, K.; Gmyrek, Z.; Szulakowski, J. The Effect of Sample's Dimension and Cutting Technology on Magnetization and Specific Iron Losses of FeSi Laminations. *Energies* **2022**, *15*, 2086. [[CrossRef](#)]

Disclaimer/Publisher's Note: The statements, opinions and data contained in all publications are solely those of the individual author(s) and contributor(s) and not of MDPI and/or the editor(s). MDPI and/or the editor(s) disclaim responsibility for any injury to people or property resulting from any ideas, methods, instructions or products referred to in the content.